

Hole quality improvement in CFRP/Ti6Al4V stacks using optimised flow rates for LCO₂ and MQL sustainable cooling/lubrication

I. Rodriguez^{a,b,*}, P.J. Arrazola^a, M. Cuesta^a, F. Pušavec^b

^a Mondragon Unibertitatea, Faculty of Engineering, Loramendi 4, Arrasate-Mondragón 20500, Spain

^b University of Ljubljana, Faculty of Mechanical Engineering, Ljubljana, Slovenia

ARTICLE INFO

Keywords:

CFRP/Ti stacks
Cutting temperature
LCO₂ assisted drilling
Surface integrity
Optimisation

ABSTRACT

Carbon fibre reinforced polymer/titanium stacks (CFRP/Ti6Al4V) are employed in aeronautics due to their excellent weight-to-strength ratio and corrosion properties. However, these same material properties present challenges for hole making which cannot be solved using conventional water-based metalworking fluids (MWFs), as they cause degradation of the composite. Moreover, environmental and health concerns require exploration of alternative cooling/lubrication solutions. In this study, a controlled mixture of liquid carbon dioxide (LCO₂) and minimum quantity lubrication (MQL) was supplied through the drilling tool. The effect of varying LCO₂ and MQL flow rates was evaluated on cutting forces, temperatures, and several hole quality outputs. The optimal flow rates were then determined through multi-objective optimisation. The results show that the cooling/lubrication flow rate greatly affects the measured outputs, and that supplying LCO₂ + MQL with optimised flow rates helps achieve superior quality holes in CFRP, Ti6Al4V and CFRP/Ti6Al4V stacks.

1. Introduction

The European aviation industry is committed to reach net zero CO₂ emissions from all flights departing from the EU by 2050 [1]. One possible pathway to achieve this is to reduce fuel consumption by reducing take-off weight. Consequently, multilayer composite/metal stacks have been increasingly used in the manufacture of aircraft structural components, due to their high weight-to-strength ratio, corrosion resistance, and thermal stability. Carbon fibre reinforced polymers (CFRP) and alpha/beta titanium alloys, like Ti6Al4V, are two representative materials used to produce these sandwich materials. In modern aircrafts, as the Airbus A350 and Boeing 787 Dreamliner, these materials are found in stacked configuration in some parts of the fuselage, central wing box, and wing spar panels [2].

Rivets or screws are typically used to join composite and metal components and form stacks in aerospace structural applications, making mechanical drilling an essential machining operation in the aerospace industry [3]. Drilling CFRP and Ti6Al4V plates in one operation reduces positioning errors and cycle times. However, the disparate nature of the materials lead to machinability and hole quality issues. The abrasive carbon fibres wear down the tool coating [4] increasing the risk of adhesion wear when machining the Ti6Al4V phase [5]. This

combined abrasive and adhesive wear increases the tool wear rate compared to drilling both materials separately [2,3].

Hole defects when drilling CFRP/Ti6Al4V stacks depend on the drilling direction. Xu et al. have demonstrated experimentally [3] and using finite element method (FEM) simulations [6] that the drilling from CFRP to Ti6Al4V produces the best quality holes. Yet, even in this drilling order, several hole quality issues persist (Fig. 1a). For instance, peel-up delamination appears at the entrance of the CFRP phase as the rake face of the drill pulls up the first plies of the laminate like a cork-screw [2,4]. Fibre pull-out also occurs in the machined surface, as both the flutes of the drill bit and the titanium chips being evacuated pull out fibre bundles as the hole is drilled [7]. Additionally, the heat generated when drilling Ti6Al4V (about 500 °C at the tool lip at $V_c = 30$ m/min in dry [8]), can lead to carbonisation of the composite matrix at the interface region as it exceeds its glass transition temperature (180 °C) [9,10]. Drilling induced defects in the Ti6Al4V phase include poor surface roughness and excessive burr height. These problems can affect component mechanical properties and aircraft part assembly, resulting in the need to re-machining or rejecting parts.

Various solutions have been explored to overcome these machinability and hole quality issues [11]. For instance, special tool geometries (Fig. 1b) that minimise thrust force and thus the drilling induced

* Corresponding author.

E-mail address: irodriguez@mondragon.edu (I. Rodriguez).

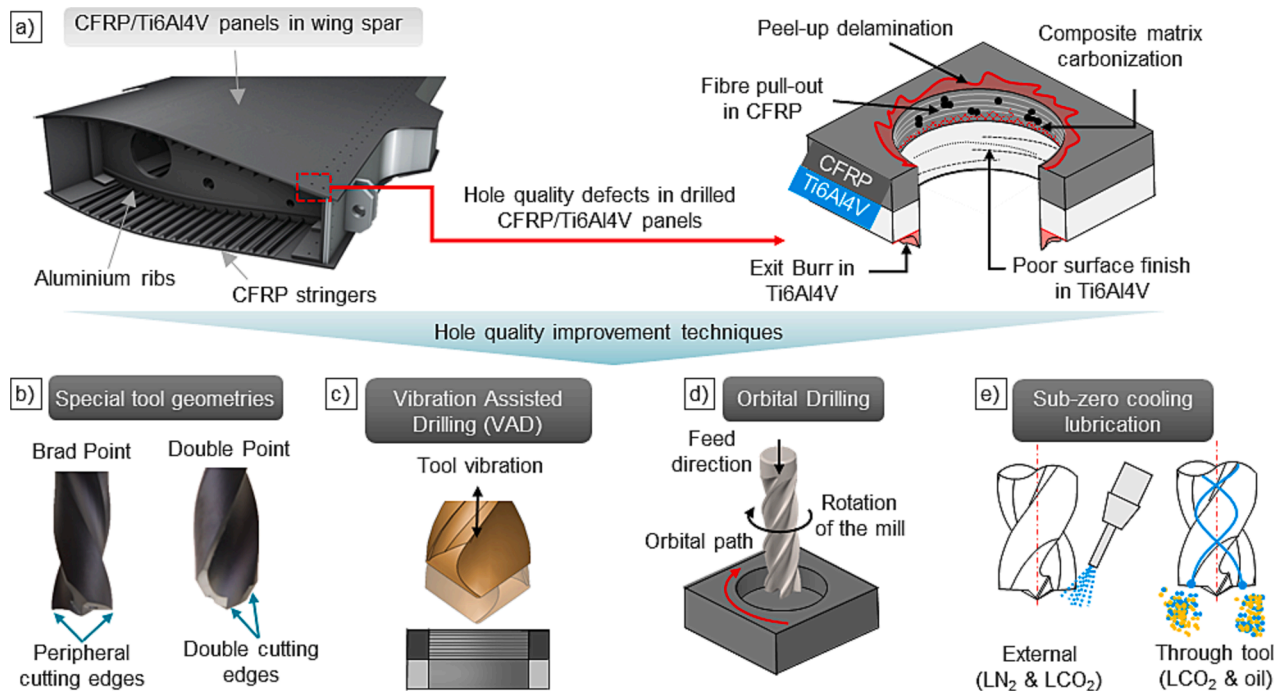


Fig. 1. Overview of advances in mechanical drilling of CFRP/Ti6Al4V stacks: a) Applications and hole quality defects; b) – e): Most common hole quality improving techniques.

Table 1

Summary of the outputs measured by the most relevant studies concerning drilling of CFRP and Ti6Al4V materials employing techniques to suppress machinability and hole quality problems.

Study	Technique	Material	Forces	Temperature	Hole quality		
					Hole entry/exit (Delamination, burr height etc.)	Hole surface (Fibre pull-out, surface roughness, etc.)	Dimensional accuracy (Diameter, roundness)
[40]	Vibration assisted drilling	CFRP	✓	✓	✓	✓	–
[41]	Vibration assisted drilling	CFRP	✓	–	✓	✓	✓
[39]	Vibration assisted drilling	Ti6Al4V	✓	–	✓	–	–
[7]	Vibration assisted drilling	CFRP/Ti6Al4V stack	–	✓	✓	✓	✓
[42]	Vibration assisted drilling	CFRP/Ti6Al4V stacks	✓	✓	✓	✓	–
[43]	Vibration assisted drilling	CFRP/C45E stack	✓	–	–	✓	–
[10]	Vibration assisted drilling	CFRP/Ti6Al4V stack	✓	✓	✓	✓	✓
[13]	Vibration assisted drilling	CFRP/Ti6Al4V stack	✓	✓	✓	✓	✓
[14]	Vibration assisted drilling	CFRP/Ti6Al4V stack	✓	✓	–	–	–
[15]	Orbital drilling	CFRP	✓	✓	–	✓	✓
[44]	Orbital drilling	CFRP/Ti6Al4V stack	✓	–	–	–	✓
[45]	Orbital drilling	CFRP	✓	✓	✓	–	–
[46]	MQL	CFRP/Ti6Al4V stack	✓	–	✓	✓	✓
[47]	MQL	CFRP/Ti6Al4V stack	✓	–	✓	✓	✓
[48]	MQL	CFRP/Ti6Al4V stack	–	–	✓	✓	✓
[19]	LN ₂	CFRP	✓	–	✓	–	✓
[20]	LN ₂	Ti6Al4V	✓	–	–	–	✓
[49]	LN ₂	CFRP and Ti6Al4V (separately)	✓	–	–	✓	–
[5]	LN ₂ and LCO ₂ (separately)	Ti6Al4V	✓	–	–	✓	✓
[18]	LCO ₂	Ti6Al4V	✓	✓	–	✓	–
[50]	LCO ₂	CFRP/Ti6Al4V stack	–	✓	✓	–	✓
[23]	LCO ₂ + lubricant media	CFRP and Ti6Al4V (separately)	✓	–	✓	✓	–

delamination in composite materials [12]. Brad point and double point angle tools are the most popular, and are even commercially available (SECO FeedMax drills for CFRP/Ti6Al4V stacks). Brad point tools reduce the thrust force thanks to peripheral cutting edges, while double point angle tools have a small point angle at the secondary stage which helps to minimise delamination in the composite and reduce the length of metal chips due to a change in chip flow direction through the double

cutting edges [4]. These tools can also be made from super-hard materials such as polycrystalline diamond (PCD), or diamond coated tungsten carbide to resist the abrasive wear from the hard reinforcement fibres.

Techniques which focus on improving chip evacuation, such as vibration assisted drilling (VAD, in Fig. 1c) and orbital drilling (OD, in Fig. 1d), have been also widely studied for improving hole quality in

CFRP/Ti6Al4V stacks. In VAD a periodic displacement is applied to the tool to promote discontinuous chip formation, in turn the drilling temperature and the mechanical abrasion and thermal damage produced by titanium chips on the CFRP phase are reduced [10,13,14]. OD on the other hand, consists of using a milling tool with a diameter smaller than the hole following a helical trajectory. This improves chip evacuation and lowers the cutting temperature. The axial load is also reduced, as the larger force component is directed in the tangential direction, reducing CFRP delamination [15].

Metalworking fluids (MWFs) are also used to reduce temperature and improve chip evacuation and lubrication when cutting a wide range of materials. Nevertheless, conventional oil and water-based MWFs are unsuitable for drilling CFRP/Ti6Al4V stacks, since the moisture absorption by the composite can cause swelling and degradation of matrix-reinforcement bond [16]. Additionally, conventional MWFs can cause various environmental and health risks, such as skin diseases and respiratory problems [17]. Alternatives like minimum quantity lubrication (MQL), or the use of liquefied gases, namely liquid nitrogen (LN₂) or liquid carbon dioxide (LCO₂) have been researched for drilling CFRP/Ti6Al4V stacks (Fig. 1e). MQL is the most researched technique, as it is easier to implement in machine-tools than cooling using liquefied gases. The main disadvantage of MQL is its low heat extraction capacity, but this could be improved up to three times by combining it with sub-zero liquefied gases, as proven by Jamil et al. [18]. LN₂ has proven to reduce the thermal damage and increase hole accuracy when drilling CFRP [19] as well as Ti6Al4V [20], due to its cold temperature (-197 °C). On the downside, since LN₂ needs to be kept at -197 °C and at ambient pressure, storing and/or delivering it through the tool are major technical challenges. LCO₂, on the other hand, can be stored at room temperature and a pressure of 57 bar, which gives rise to the possibility of mixing it with lubricating oils or delivering it through the machine spindle. When LCO₂ is rapidly expanded to ambient pressure, its temperature instantly drops to -79 °C [21]. The relative ease of storage and management of LCO₂, and the ability to mix it with lubricating oils or deliver it through the spindle has motivated the development of industrial-grade LCO₂ cooling/lubrication solutions [22].

Table 1 summarizes the main studies in which the techniques described previously have been used to overcome tool life and hole quality problems when drilling CFRP/Ti6Al4V stacks. Most studies conclude that drilling from a CFRP to Ti6Al4V direction provides the best hole quality results, provided that sufficient titanium chip evacuation is ensured. VAD, OD and MQL lubrication are the most widely researched techniques for CFRP/Ti6Al4V stacks. While LN₂ and LCO₂ cooling has been mostly studied for drilling CFRP and Ti6Al4V separate plates, there is little published data on LCO₂ + MQL cooling/lubrication for drilling stacked aeronautical materials (Table 1).

Regarding the outputs, few studies exist that monitor the cutting temperature throughout the entire cutting process. Additionally, apart from the studies by Xu et al. [10] and Hussein et al. [13], there is a lack of research works that provide a comprehensive assessment of the drilled hole quality, and link those results to cutting forces and temperature.

Therefore, the present work aims to optimise LCO₂ + MQL delivery to ensure the best hole quality when drilling CFRP, Ti6Al4V and CFRP/Ti6Al4V stacks. For this purpose, a sensitivity analysis of independently varying the LCO₂ and MQL flow rates (q_{LCO_2} and q_{MQL}) was carried out on cutting forces and temperatures. The analysis also considered several hole quality defects, such as delamination (push-out for individual CFRP plates and peel-up for CFRP/Ti6Al4V stacks), fibre pull-out, and epoxy matrix carbonisation for CFRP, as well as surface roughness and burr height for Ti6Al4V. Dimensional accuracy (hole diameter and roundness) was monitored at different heights for each material.

A multi-objective optimisation (MOO) was conducted with the monitored outputs for CFRP, Ti6Al4V and CFRP/Ti6Al4V stacks (the measured hole quality parameters varied depending on the workpiece material) to determine the optimal LCO₂ and MQL cooling and

lubrication flow rates (q_{LCO_2} and q_{MQL}) for drilling each material. To reduce the experimental campaign, an initial series of tests consisting of 16 different q_{LCO_2}/q_{MQL} combinations was tested on separate CFRP and Ti6Al4V plates, and the optimal cooling/lubrication flow rates were employed to define the input conditions for the CFRP/Ti6Al4V stack drilling experiments.

The results discussed in this paper help to define a process window for drilling CFRP/Ti6Al4V stacks with LCO₂ based cooling/lubrication to improve the resulting quality of the part and minimise the mechanical and thermal loads on the tool. This study also adds to the knowledge of heat generation when drilling composite/metal stacks under dry and sub-zero cooling/lubrication.

2. Tools and materials

A Brad point tool (SECO SD205A-6.0-32-6R1-C2) with internal cooling channels specially designed for through the tool LCO₂ delivery was used for the tests. This tool geometry minimises defects in one of the most crucial parts of composite/metal stacks, which is peel-up delamination at the entry plane of the composite. By having a tip angle of 180° at the periphery, the forces get distributed in the axial direction, pushing down the fibres at the entrance, and preventing delamination. Additionally, SECO Brad point drill bits proved suitable to machine Ti6Al4V with minimal microstructural damage [23]. The tools also have a

Table 2
Geometrical parameters of the Brad point drill.

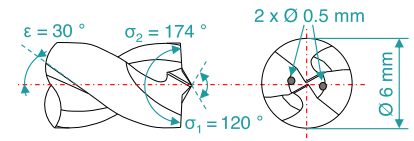
Reference	SD205A-6.0-32-6R1-C2
Target material	CFRP/Ti6Al4V stacks (CFRP to Ti6Al4V)
Coating	Diamond CVD
Point angle, σ [°]	120/174
Diameter, ϕ [mm]	6
Coolant channels	2 × ϕ 0.5 mm
Edge radius, r_c [μ m]	11 ± 2
Wedge angle, β [°]	43.9 ± 5.8
Tool geometry	

Table 3
Mechanical properties of reinforcement fibres and epoxy matrix of the aeronautical grade CFRP composite at room temperature.

Reinforcement fibres	Reference	Sigatex CW205 TW2/2
	Areal weight [g/m ²]	205
	Tensile strength [MPa]	2400
	Tensile Modulus [GPa]	300
	Fibre volume [%]	50
Epoxy matrix	Reference	Hexcel Hexflow RTM 6-2
	Tensile strength [MPa]	75
	Tensile Modulus [GPa]	2.9
	Strain [%]	3.4
	Density [g/cm ³]	1.14

Table 4
Chemical composition (% by weight) and mechanical properties of the Ti6Al4V alloy, at room temperature.

Chemical composition	Fe	0.15
	V	4.14
	Al	6.50
	C	0.003
	O	0.18
	N	0.004
Mechanical properties	Y	< 0.001
	Tensile strength, Yield [MPa]	Long.: 921; Trans.: 967
	Tensile strength, ultimate [MPa]	Long.: 973; Trans.: 967
	Elongation [%]	Long.: 12.5; Trans.: 15

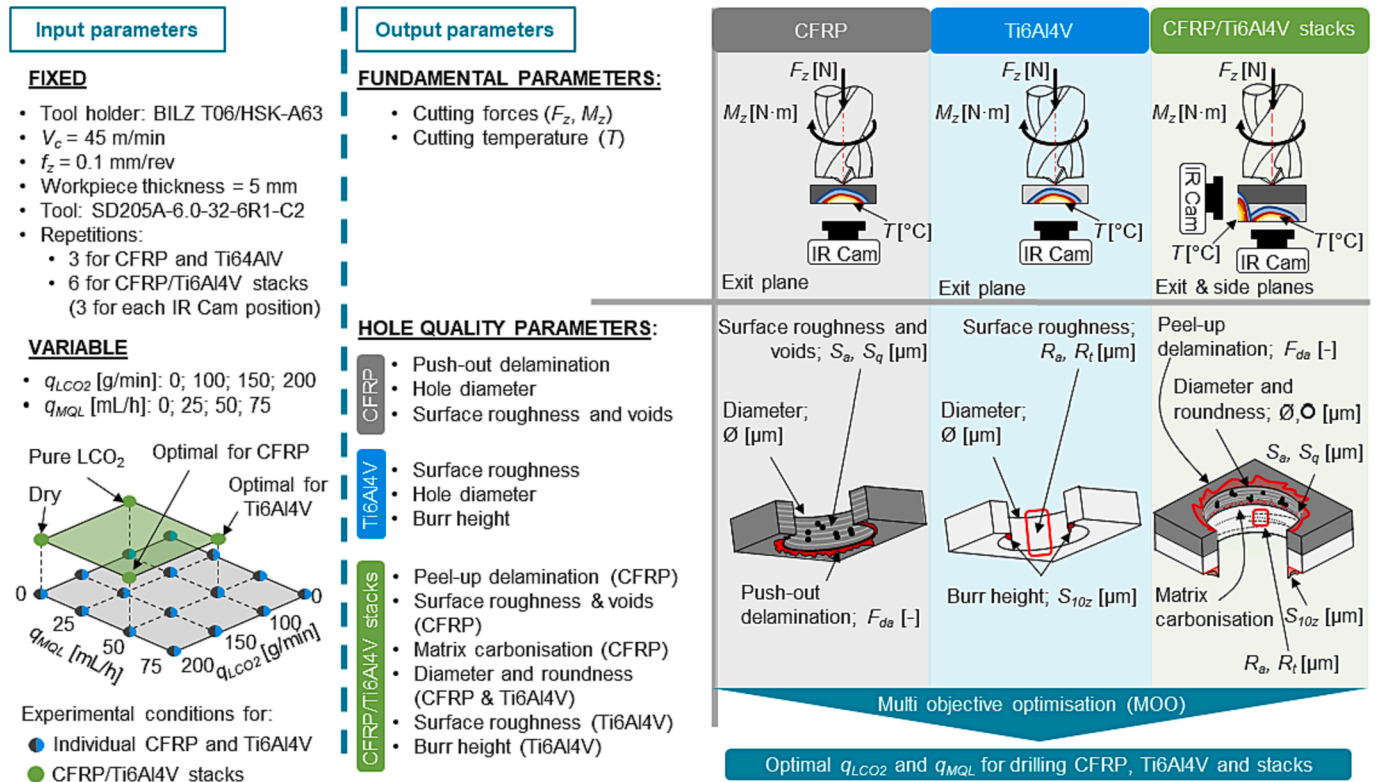


Fig. 2. Scheme of the experimental procedure carried out: input parameters and output parameters monitored for the MOO in CFRP Ti6Al4V and CFRP/Ti6Al4V stacks.

Table 5
Output parameters analysed in the study for different workpiece materials.

Output parameter	CFRP	Ti6Al4V	CFRP/Ti6Al4V stacks
Thrust force, F_z	✓	✓	✓
Torque, M_z	✓	✓	✓
Temperature, T	✓	✓	✓
Hole diameter, \varnothing	✓	✓	✓
Roundness, \circ	-	-	✓
Arithmetic mean height, S_a	✓	✓	✓
Maximum valley depth, S_v	✓	-	✓
Delamination, F_{da}	✓(Push-out)	-	✓(Peel-up)
Matrix carbonisation	-	-	✓
Average surface roughness, R_a	-	✓	✓
Maximum peak to valley height, R_t	-	✓	✓
Ten point burr height, S_{10z}	-	✓	✓
LCO ₂ flow rate, q_{LCO2}	✓	✓	✓
MQL flow rate, q_{MQL}	✓	✓	✓

Table 6
Cutting forces and temperatures acquisition details.

Forces	Equipment	Kistler 9273
	Acquisition rate [Hz]	2400
	Filter	Low pass at 150 Hz
Temperature	Equipment	Telops Fast M3k
	Temperature ranges [°C]	0 to 185; 114 to 377; 254 to 680
	Image format [pixel]	256 × 320
	Spatial resolution [µm/pixel]	180
	Acquisition rate [Hz]	1200
	Exposure time [µs]	CFRP: 25 Ti6Al4V: 4
	Reflected temperature [°C]	21.5
	Emissivity, ϵ [%]	85

Chemical Vapour Deposition (CVD) diamond coating to resist the abrasion caused by carbon fibres, and a cutting edge radius of $11 \pm 2 \mu\text{m}$. The cutting edge of the tools was characterized using an Alicona Infinite Focus SL optical 3D microscope, using the rotation unit with a $\times 10$ magnification, to obtain the 3D geometry of the tool. The main geometric features of the tool are summarised in Table 2.

CFRP and Ti6Al4V plates of the same dimensions ($40 \times 250 \times 5 \text{ mm}^3$) were used for the experiments. The CFRP plates were fabricated using aeronautical grade carbon fibre reinforcement fibres and epoxy resin and a Resin Transfer Moulding (RTM) press. 20 layers of reinforcement were used per plate to achieve a 50% fibre volume and the mould was pressed at 5 Tn and 140°C for 180 min to cure the resin. After the epoxy cured, a post-curing treatment was performed in an oven at 180°C for 2 h. The mechanical properties of the CFRP plates are summarized in Table 3 and those of Ti6Al4V in Table 4.

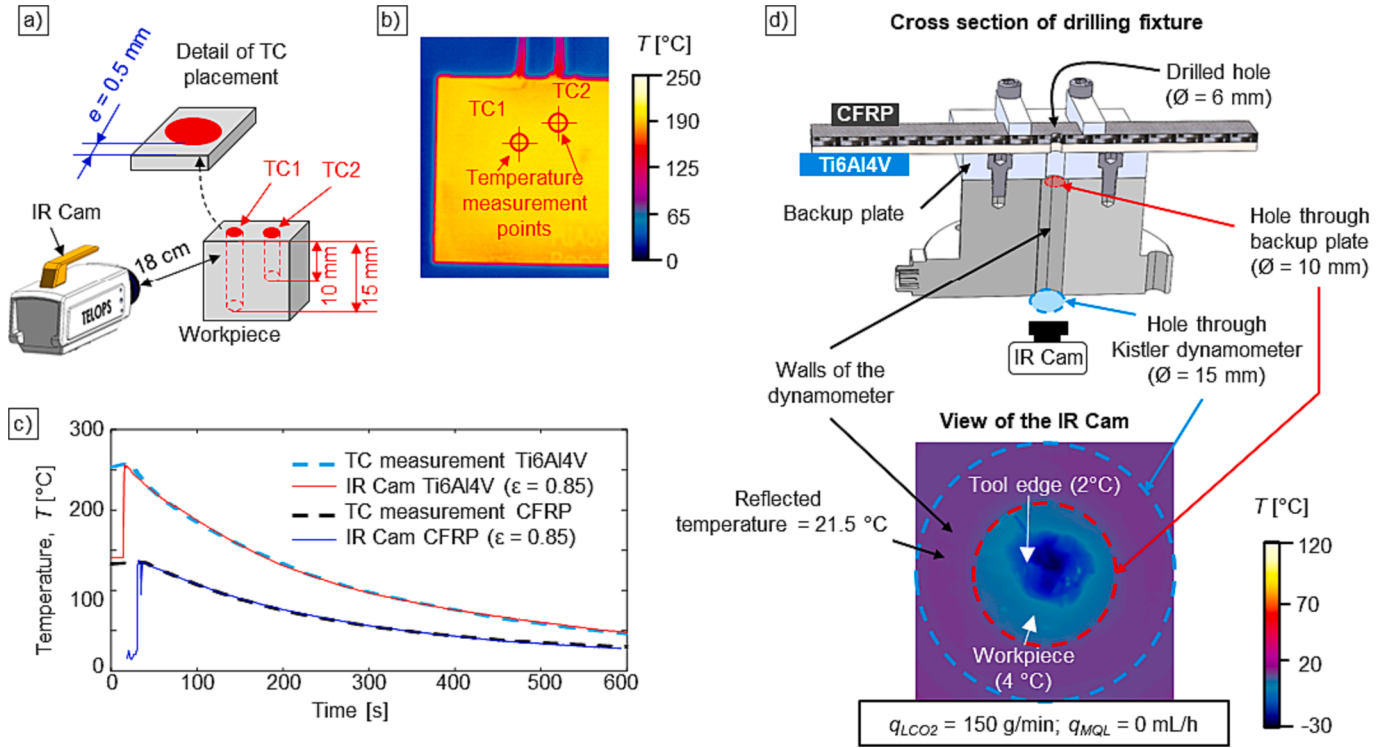


Fig. 3. Temperature calibration procedure: a) Calibration setup; b) Thermal field measurements of the workpiece acquired with the infrared camera; c) Temperature drop measured using the thermocouples and infrared camera with calibrated emissivity; d) Calibration of the reflected temperature.

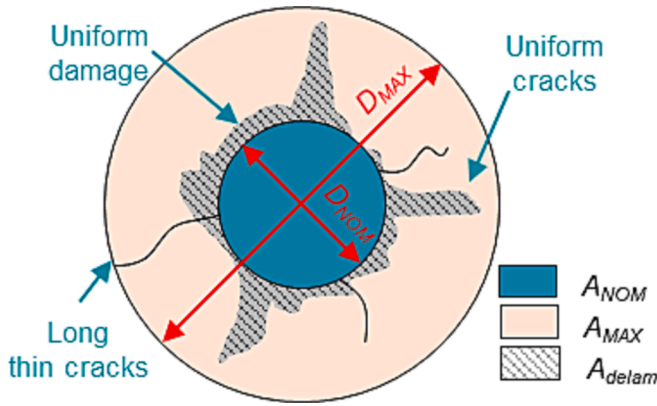


Fig. 4. Advanced delamination factor (F_{da}) proposed by Davim et al. [32].

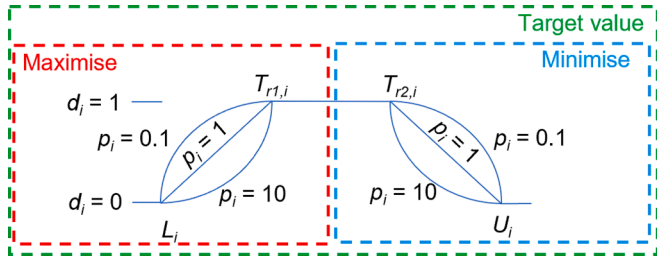


Fig. 5. Representation of individual desirability function.

3. Methodology

3.1. Experimental plan

Fig. 2 summarizes the fixed and variable inputs employed in the experiments carried out on individual CFRP and Ti6Al4V plates and CFRP/Ti6Al4V stacks, as well as the outputs monitored for each material. The experimental campaign was divided into two stages: (i) cooling/lubrication flow rate optimisation for drilling individual CFRP and Ti6Al4V plates, and (ii) cooling/lubrication flow rate optimisation for drilling CFRP/Ti6Al4V stacks.

The tool geometry described in section 2, cutting parameters ($V_c = 45$ m/min; $f_z = 0.1$ mm/rev recommended by SECO Tools), and workpiece dimensions were fixed for all experiments. The MQL oil used was Rhenus Lub SSM neat oil (viscosity 3.5 mm²/s at 20 °C), which ensures good mixing with LCO₂, as demonstrated by [21,24]. For the cases in which only MQL was delivered, the oil was supplied to the cutting zone using room temperature gaseous CO₂ as the carrier medium at a flow rate of 10 g/min. The variable input parameters and monitored output parameters varied depending on the drilled workpiece material. These are detailed in the following subsections.

To minimise the effect of tool wear on the evaluated outputs a new tool was used after a certain number of holes for each material (25 for CFRP, 16 for Ti6Al4V, and 12 for CFRP/Ti6Al4V stacks). The tools were checked regularly between tests for signs of wear on the chisel or peripheral cutting edges.

3.1.1. Experiments in individual CFRP and Ti6Al4V plates

As Fig. 2 shows, 16 LCO₂ and MQL flow rates (q_{LCO_2} and q_{MQL}) were tested for individual CFRP and Ti6Al4V plates (black and blue dots). Each experimental condition was repeated three times to determine the uncertainty. The output parameters evaluated for individual plate drilling experiments are schematically shown in the black (CFRP) and blue (Ti6Al4V) columns in Fig. 2. Cutting forces and the temperature at the exit plane were measured for both materials. Regarding the hole quality,

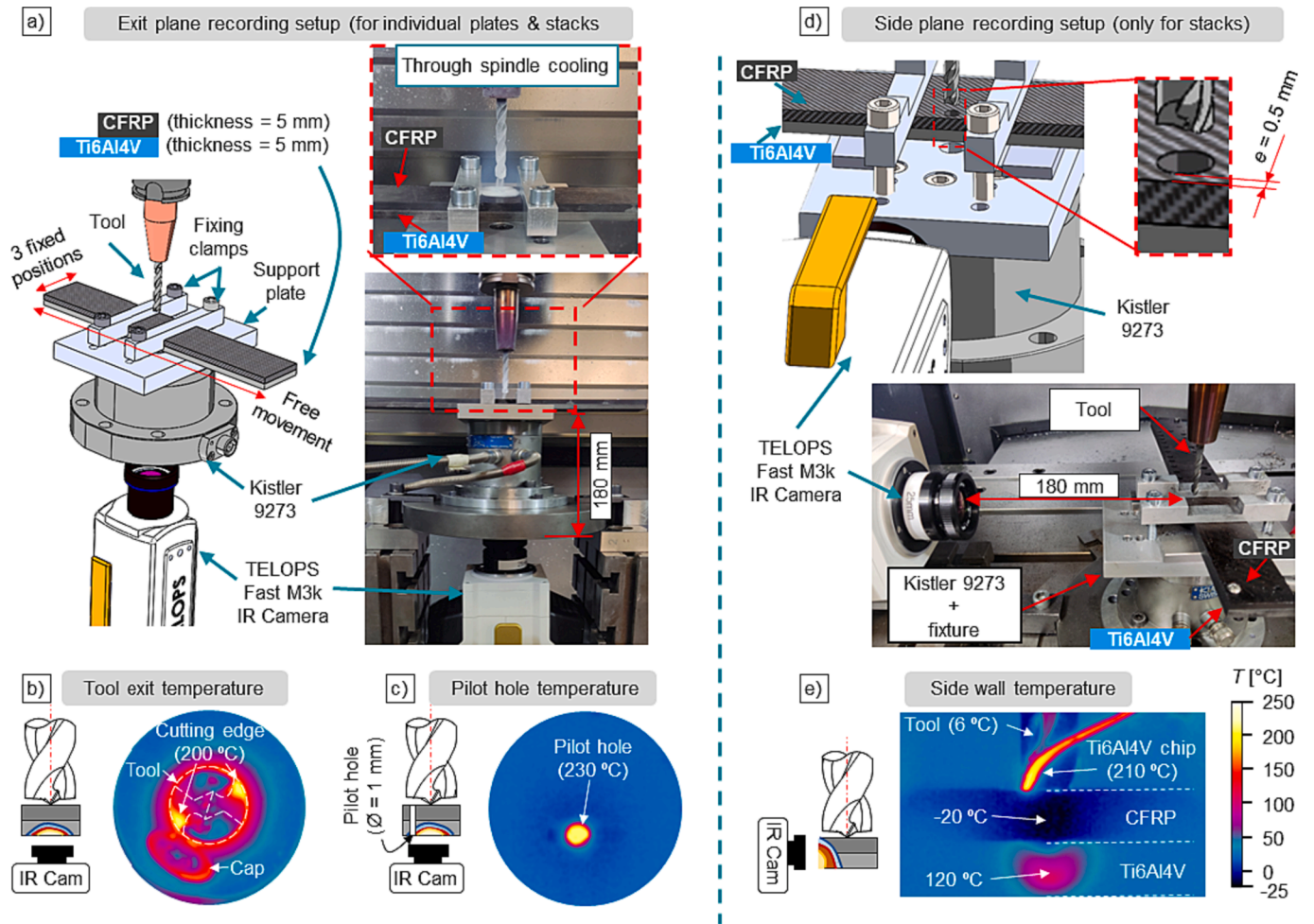


Fig. 6. Different setups employed in the experiments: a) Layout for tool exit and pilot hole temperature recording; b) Temperature fields when recording the exit plane; c) Temperature fields when recording through pilot hole; d) Layout for side wall temperature recording; e) Temperature fields when recording from the side plane.

the diameter was evaluated both for CFRP and Ti6Al4V plates, however, different parameters were measured to assess the quality of the machined surface and the defects at the exit plane of the hole depending on the workpiece material.

For instance, when drilling Ti6Al4V the burr height was measured at the exit plane using the ten-point height (S_{10z}) parameter, in order to reduce the uncertainty of irregular burrs [25]. The surface roughness parameters measured were those which define fatigue strength (average surface roughness, R_a and maximum peak to valley height, R_t) [26]. Unfortunately, the roughness parameters measured to evaluate the quality of the machined titanium surface cannot be used for CFRP. The coexistence of reinforcement fibres and epoxy resin makes the machined surface inhomogeneous, and evaluating the surface roughness through profiles becomes difficult, since the results vary depending on the position and orientation of the profile. Duboust et al. [27] showed in their study that the arithmetic mean height of area roughness (S_a), and the maximum valley depth (S_v) surface texture parameters accurately represent the average roughness of the surface and the presence of voids due to fibre pull-out on the machined CFRP surface. Therefore, in the present research, S_a and S_v were measured to evaluate the surface quality. No burr is formed when drilling CFRP, however the composite plies are usually delaminated, and hence, push-out delamination was evaluated to assess the quality of the hole at the exit plane.

In addition to all these outputs, the LCO₂ and MQL consumption of each experimental condition were also considered to perform a multi-objective optimisation (MOO) using the response surface method

(RSM). This helped to obtain the q_{LCO_2} and q_{MQL} combination that ensured the optimal overall value of the output responses, while ensuring minimal LCO₂ and MQL consumption. The optimized q_{LCO_2} and q_{MQL} values for drilling CFRP and Ti6Al4V were employed as input values for the set of experiments on CFRP/Ti6Al4V stacks, to reduce the number of experimental runs. The output parameters taken into consideration for the CFRP and Ti6Al4V individual plate drilling experiments are listed in Table 5.

3.1.2. Experiments in CFRP/Ti6Al4V stacks

For the stack drilling experiments, a drilling direction from CFRP to Ti6Al4V was chosen as recommended by SECO Tools and studies from literature [3,6]. In addition to the optimised q_{LCO_2} and q_{MQL} values for drilling separate CFRP and Ti6Al4V plates obtained in the first experimental stage (section 3.1.1), two more cooling/lubrication conditions were tested for CFRP/Ti6Al4V stack drilling, namely dry cutting, and pure LCO₂ cooling (green dots in Fig. 2). Since fewer cooling/lubrication conditions were tested out in CFRP/Ti6Al4V stacks (four conditions) than in individual plates (16 conditions), the MOO was performed by comparing all output results, without using RSM.

Additionally, a more comprehensive temperature analysis was carried out for CFRP/Ti6Al4V stack drilling, which recorded the cutting temperature from two different positions as it is shown in the green column in Fig. 2: (i) from the exit plane, recording the temperature through a pre-drilled 1 mm pilot hole eccentric to the drill bit axis, and (ii) from the side plane, following the studies by [10,13,14,28].

Therefore, each experimental condition was repeated six times (three for each camera position).

The hole quality analysis for drilled CFRP/Ti6Al4V specimens was also more detailed than for separate plates, as the roundness was measured in addition to the hole diameter. Also, as the CFRP was supported by the Ti6Al4V, the delamination only occurred at the entry plane (peel-up delamination). The defect measured at the exit plane of the CFRP was the matrix carbonisation generated by the heat of the titanium plate under the CFRP phase. Burr height (S_{10z}) and machined surface morphology parameters (S_a , S_v for CFRP and R_a , R_t for Ti6Al4V) were measured same as in the individual plate experiments. The output parameters monitored for CFRP/Ti6Al4V stack drilling are summarized in Table 5.

3.2. Evaluation of output parameters

3.2.1. Cutting forces and temperature

The detailed parameters for the force and temperature acquisition systems can be found in Table 6. Thrust force and torque values were measured with a Kistler 9273 dynamometer. The cutting force signals were filtered with a 150 Hz low-pass filter, since the first natural damped frequency of the workpiece clamping system is 1500 Hz and we applied a filter at 10% of this frequency. The temperature during the drilling process was recorded using a Telops Fast M3k high speed infrared camera (IR Cam), at a frame rate of 1200 Hz. The thermal imaging equipment was calibrated using the Telops blackbody free calibration technique [29] to minimise the effects of the surrounding environment. However, it is known that the accuracy of thermal imaging can be affected by numerous factors such as the workpiece material, and even the ambient temperature [30]. When the temperature desired to measure is close to the ambient one, the radiation emitted by surrounding objects can affect the readings by the IRCam, therefore the reflected temperature must be properly characterised [31].

The emissivity calibration of the CFRP and Ti6Al4V materials was carried out following the study of Segurajauregui et al. [28]. The workpieces were painted with a heat resistant black spray to minimise reflection, and two K-Type thermocouples (TC) (ElPro NiCr-Ni-K) were embedded at two different depths and a distance of 0.5 mm from the surface (Fig. 3a). Then, the temperature readings of the TCs were compared to those of the IR Cam at the position of the TC tip (Fig. 3b), and the emissivity of the camera was varied until the temperature readings matched those of the TCs. The camera lens was placed at a distance of 180 mm from the workpiece, similar position to the drilling experiments. The CFRP samples were heated up to 140 °C to avoid damaging the epoxy matrix, while the Ti6Al4V samples were heated up to 260 °C (maximum temperature of the furnace). The temperature change due to conductivity across the 0.5 mm of material between the surface of the workpiece and the position of the TC was taken into account. The temperature readings did not change for different depths of the TC. As seen in Fig. 3c an emissivity of $\varepsilon = 0.85$ matched best the temperature of the thermocouple inserted into the CFRP and Ti6Al4V specimens painted in black. Regarding the reflected temperature, it was calibrated for every experiment following the diffuser reflector method [31]. The drilled workpiece was employed as the heating source, and the reflection in the dynamometer walls was used to estimate the reflected temperature (Fig. 3d). A value of 21.5 ± 1.5 °C was measured in all experiments where the cutting temperature was lower than 120 °C.

3.2.2. Hole quality parameters

As described in subsection 3.1 defects at the entry and exit planes of the hole (peel-up and push-out delamination, matrix carbonisation, burr height and hole diameter and roundness) were characterised depending on the workpiece material. After that, the workpieces were cut by water jet to reveal the cross section and measure surface integrity parameters (S_a , S_v for CFRP and R_a , R_t for Ti6Al4V). The hole diameter and roundness were measured using a Renishaw Cyclone Series 2 coordinate

measurement machine. Delamination and matrix carbonisation in CFRP were observed using a Keyence VHX 6000 digital microscope with a $\times 30$ magnification. The delamination factor was evaluated following the method proposed by Davim et al. [32], since it takes into account the contribution of areal damage as well as thin cracks to the delamination. A graphical representation of the delamination factor is shown in Fig. 4, and it is calculated using the following equations, as described in [32]:

$$F_{da} = F_d + \frac{A_{delam}(F_d^2 - F_d)}{A_{MAX} - A_{NOM}} \quad (1)$$

Where,

$$F_d = \frac{D_{MAX}}{D_{NOM}} \quad (2)$$

The burr height in Ti6Al4V single plates and stacks, as well as the machined surface defects in CFRP and Ti6Al4V (both separately and in stacks) were characterised using an Alicona Infinite Focus SL 3D optical microscope with a $\times 10$ magnification.

3.3. Multi-objective optimisation

Due to the high volume of input conditions in separate CFRP and Ti6Al4V plate drilling experiments, multi-objective optimisation (MOO) using the response surface method (RSM) was carried out to determine the Q_{LCO2} and Q_{MQL} values that give the best overall results for each material. For the RSM, the regressions defining each of the response surfaces (y_i) were obtained, using a full quadratic model.

Desirability functions were calculated to optimise the response regressions. By defining the objectives and constraints of the optimisation, an individual desirability function (d_i) can be defined for each of the responses. These functions are defined as a piecewise function (Eq. (3)), and the intervals that make up the equation vary according to the objective defined for the response (maximisation, minimisation, target value). For every d_i , the lower limit value (L_i), upper limit value (U_i) and lower and upper thresholds of the target value ($T_{r1,i}$ and $T_{r2,i}$) were defined. The equation limitation levels for the different objectives are shown in Fig. 5.

$$d_i = \begin{cases} 0 & y_i < L_i \\ \frac{y_i - L_i}{T_{r1,i} - L_i} & L_i \leq y_i \leq T_{r1,i} \\ 1 & T_{r1,i} \leq y_i \leq T_{r2,i} \\ \frac{U_i - y_i}{U_i - T_{r2,i}} & T_{r2,i} \leq y_i \leq U_i \end{cases} \quad (3)$$

The output of the desirability function is a quantitative score of the individual optimisation result. The scores are arranged on values from 0 to 1 (the higher, the better). However, in order to reach MOO, the individual desirability functions must be combined into one overall desirability function, $D(y)$. The overall desirability function (Eq. (4)) is the weighted geometric desirability for each of the individual responses. In the current application, nine individual desirability functions will form the overall desirability function for each individual CFRP and Ti6Al4V plates (one per every output parameter listed in Table 5 for each material). In order to eliminate non-linearities, the target approximation relationship of all individual desirability evaluations was set as linear ($p_i = 1$). On the other hand, the weights (w_i) used to calculate the overall desirability function were calculated using the Entropy Weighting Method (EMW) explained by Kumar et al. [33]. The EMW enables to determine the objective weights of the responses by calculating the probability, entropy value and degree of divergence of each individual response.

$$D(y) = \left(\prod_{i=1}^n ((d_i)^{p_i})^{w_i} \right) \sum_{i=1}^n w_i \quad (4)$$

3.4. Experimental setup

Fig. 6 shows an overview of the setups created to carry out the experiments on a Doosan NX 6500 II CNC machining centre. Two different setups that allow simultaneous recording of cutting forces were employed: (Fig. 6a) positioning the camera at the exit plane (used for individual plates and CFRP/Ti6Al4V stacks), and (Fig. 6b) positioning the camera at the side plane (used for stacks only). The fixture described in Fig. 6a enabled the clamping of individual CFRP and Ti6Al4V plates and CFRP/Ti6Al4V stacks on the Kistler 9273 dynamometer. Examples of CFRP/Ti6Al4V experiments are shown in Fig. 6a, however the same fixture was employed for the experiments with CFRP and Ti6Al4V. This fixture allowed drilling in three different positions in the transversal direction, while having free movement in the longitudinal direction. The support plate had a 10 mm hole which provided homogeneous support to the workpiece, reducing the uncertainties for push-out delamination in CFRP and exit burr in Ti6Al4V, while allowing to record the temperature at the exit plane.

Positioning the camera at a distance of 180 mm from the exit plane (Fig. 6a), allowed to measure the temperature of the workpiece as the tool was exiting in individual CFRP and Ti6Al4V plate drilling experiments (Fig. 6b), as well as monitoring the temperature of the entire cutting process through an eccentric 1 mm pilot hole when drilling CFRP/Ti6Al4V stacks (Fig. 6c). A similar procedure was employed by

Ueda et al. [34], showing that is possible to record temperature of the cutting edge throughout the whole cutting process with very little effect on cutting forces. Measuring the temperature from the side plane (Fig. 6d), allowed to observe the temperature evolution on the workpiece during the cutting process (Fig. 6e). The camera was placed at 180 mm from the side of the workpiece, and the distance between the hole perimeter and the side wall of the workpiece (e) was 0.5 mm, similar to other research studies [10,13,14,28].

4. Experimental results and discussion

4.1. Individual CFRP and Ti6Al4V plates

4.1.1. Cutting forces and temperatures

The effect of varying q_{LCO_2} and q_{MQL} on the cutting forces when drilling CFRP and Ti6Al4V is shown in Fig. 7. As it can be seen an increase in q_{LCO_2} led to a rise in the thrust force (F_z) component when drilling CFRP or Ti6Al4V (Fig. 7a and b). This might be due to a rise in the flow stress of the material when being machined at colder temperatures than in dry drilling [19]. Spraying MQL on the cutting zone helped to slightly reduce the rise in F_z , however it is smaller than the increase caused by LCO_2 .

Applying MQL also helped to reduce the torque (M_z) for both CFRP and Ti6Al4V, probably due to a reduction of the friction coefficient (Fig. 7c and d). However, through the tool LCO_2 cooling brought different M_z results depending on the machined material. When drilling CFRP, an increase in q_{LCO_2} created a rise in M_z , while for Ti6Al4V case, helped to reduce it. Applying LCO_2 cooling usually increases the friction

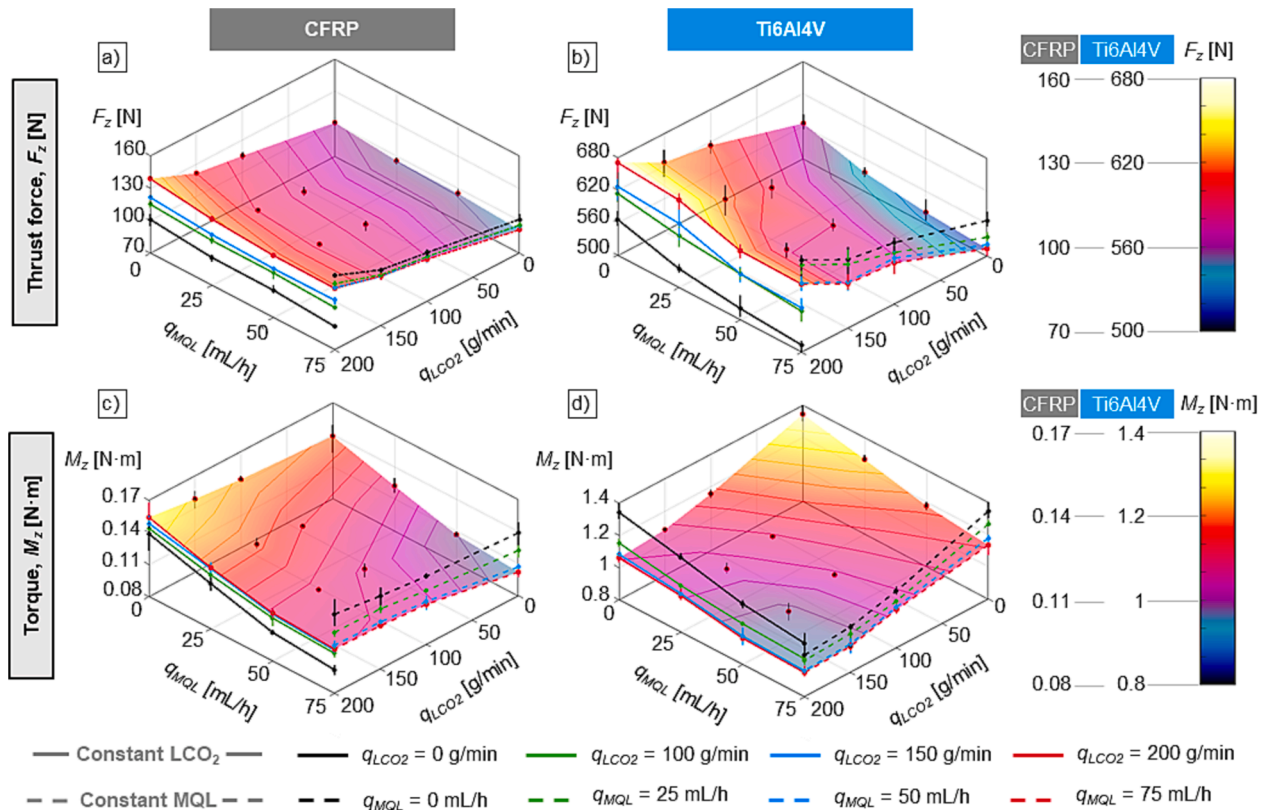


Fig. 7. Effect of varying q_{LCO_2} and q_{MQL} on cutting forces when drilling individual plates: a) Thrust force in CFRP; b) Thrust force in Ti6Al4V; c) Torque in CFRP; d) Torque in Ti6Al4V.

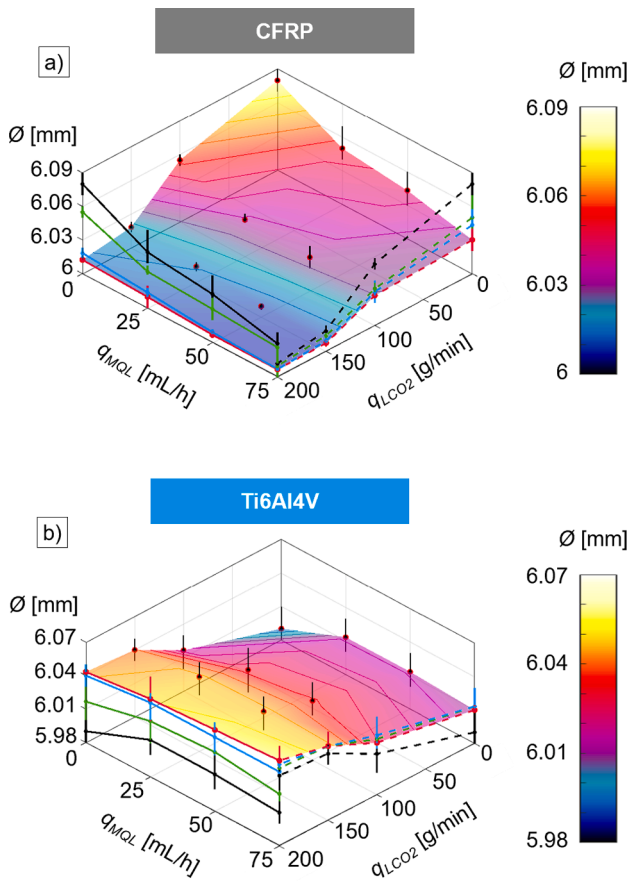


Fig. 8. Effect of varying q_{LCO_2} and q_{MQL} on hole diameter when drilling individual plates: a) CFRP; b) Ti6Al4V.

coefficient at the tool-chip interface, thus increasing the torque [35]. However, the improvement in chip evacuation generated by supplying LCO₂ through the tool at 5.7 MPa could have helped to reduce M_z when drilling Ti6Al4V [36]. The effect of torque reduction due to chip evacuation was not observed for CFRP drilling since the powder-like chips of the composite are not problematic to evacuate.

The torque generated by the tool was also affected by the hole diameter. As Fig. 8 shows, the cooling effect of LCO₂ helped to achieve holes closer to the nominal value (6 mm). This generated a reduction in M_z when drilling Ti6Al4V, since the thermal shrinkage decreases and bigger holes than in dry drilling are achieved. But on the other hand, an increase in M_z is observed when drilling CFRP, as smaller holes are machined with LCO₂ compared to dry drilling. Similar results were achieved by Xia et al. [19], who achieved holes with dimensions closer to the nominal diameter of the tool, and thus an increase in M_z when drilling CFRP with sub-zero cooling. Merzouki et al. [20] also reported that the sub-zero temperature of the coolant helped to reduce the thermal shrinkage of the hole, and hence the torque when drilling Ti6Al4V.

The cutting temperature was recorded at the exit plane of the workpiece. The key frame selected for the analysis was the previous one to the tool exit. The highest temperatures appeared during the last 50 frames before the tool exit, and the variation between them was smaller than 20 °C, as the frame rate was 1200 Hz. The response surfaces of the maximum temperatures recorded at the tool-workpiece interface when drilling CFRP and Ti6Al4V individual plates are shown in Fig. 9. The temperature fields of the key frame at constant $q_{LCO_2} = 0$ g/min and varying MQL, and constant $q_{MQL} = 0$ mL/h and varying LCO₂ are also shown for each material.

The maximum temperatures measured in dry drilling are consistent with the results of other studies, about 120 °C for CFRP [37] and 500 °C for Ti6Al4V [8]. As the cutting temperatures reached when drilling CFRP (Fig. 9a) were considerably lower than the ones for Ti6Al4V

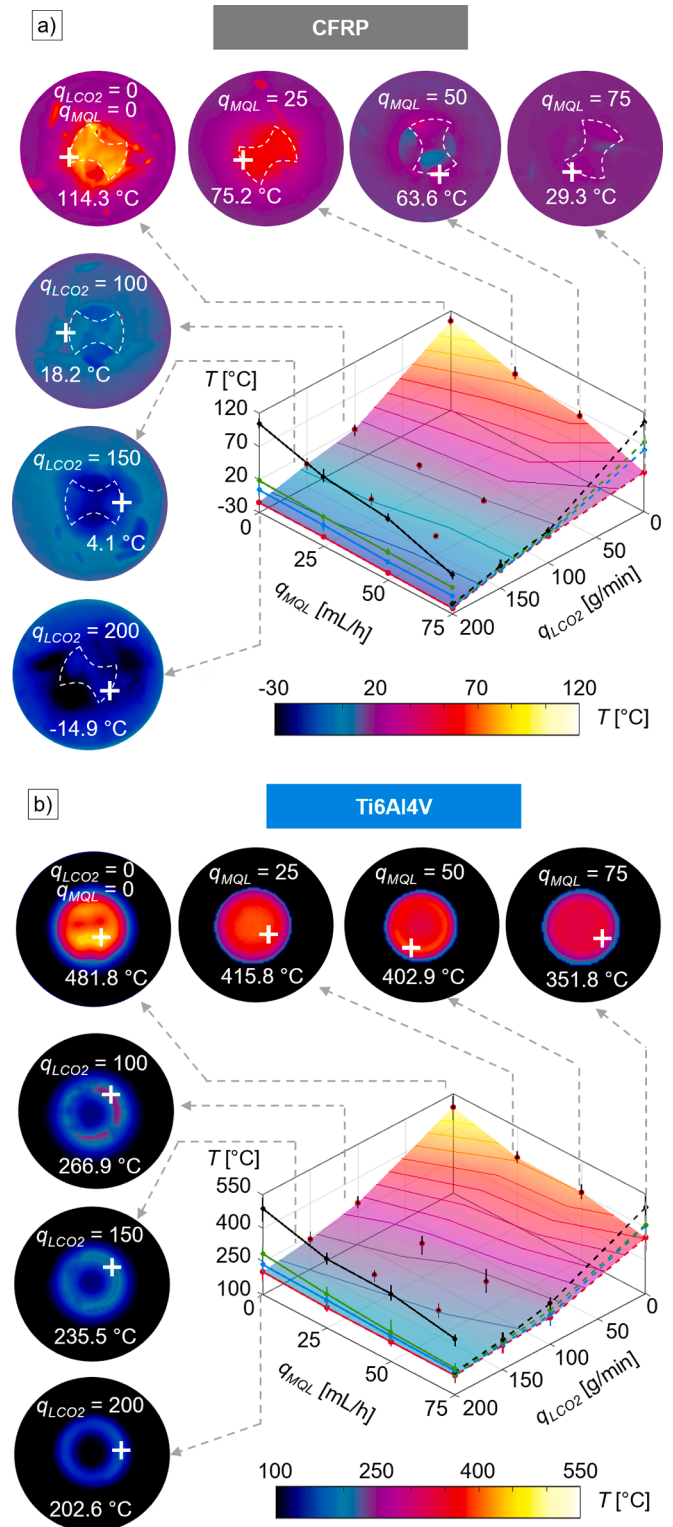


Fig. 9. Effect of varying different q_{LCO_2} and q_{MQL} on maximum temperature at the tool-workpiece interface when drilling individual plates: a) CFRP; b) Ti6Al4V.

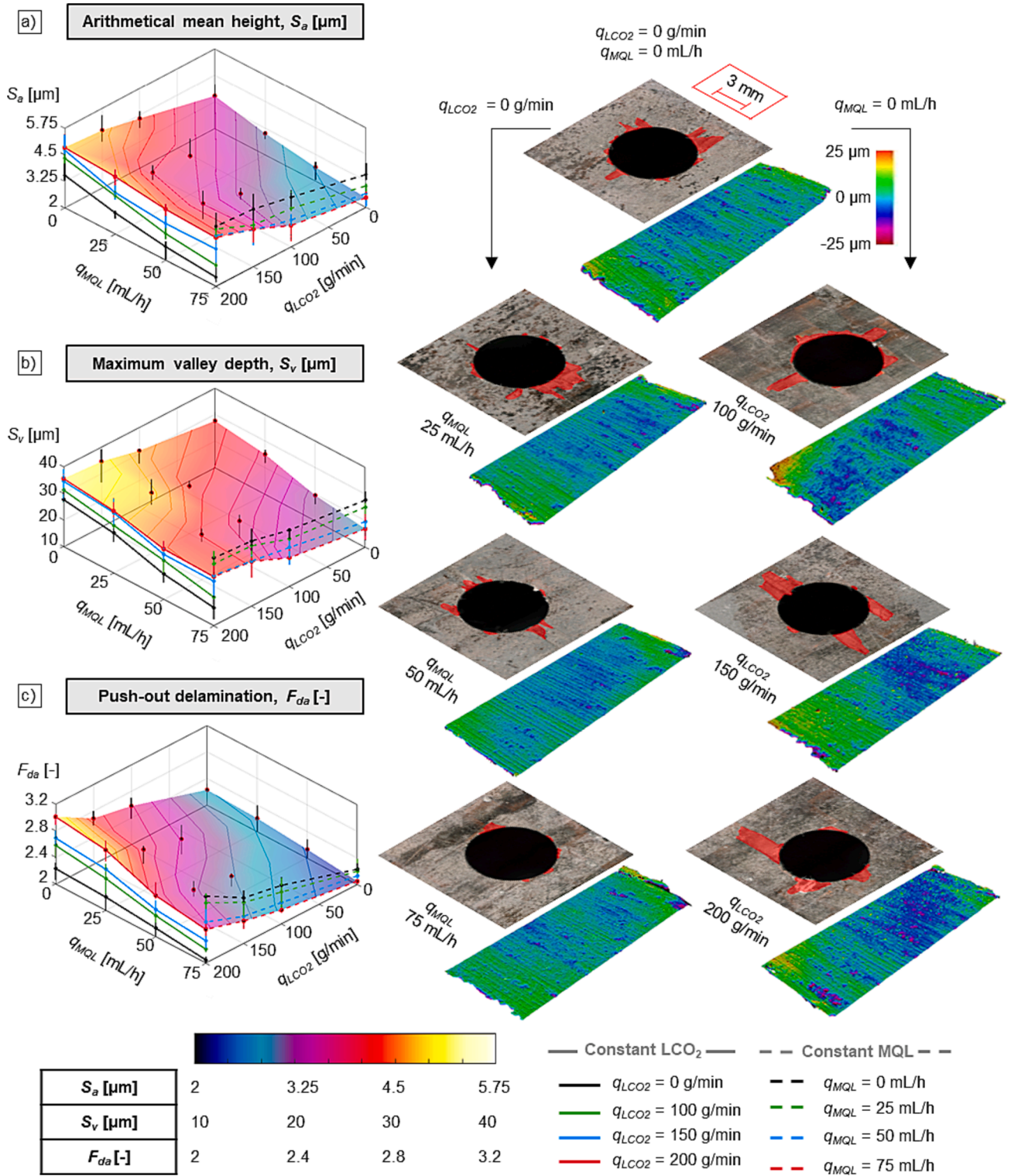


Fig. 10. Effect of varying q_{LCO_2} and q_{MQL} on hole quality when drilling CFRP individual plates: a) Arithmetical mean height; b) Maximum valley depth; c) Push-out delamination.

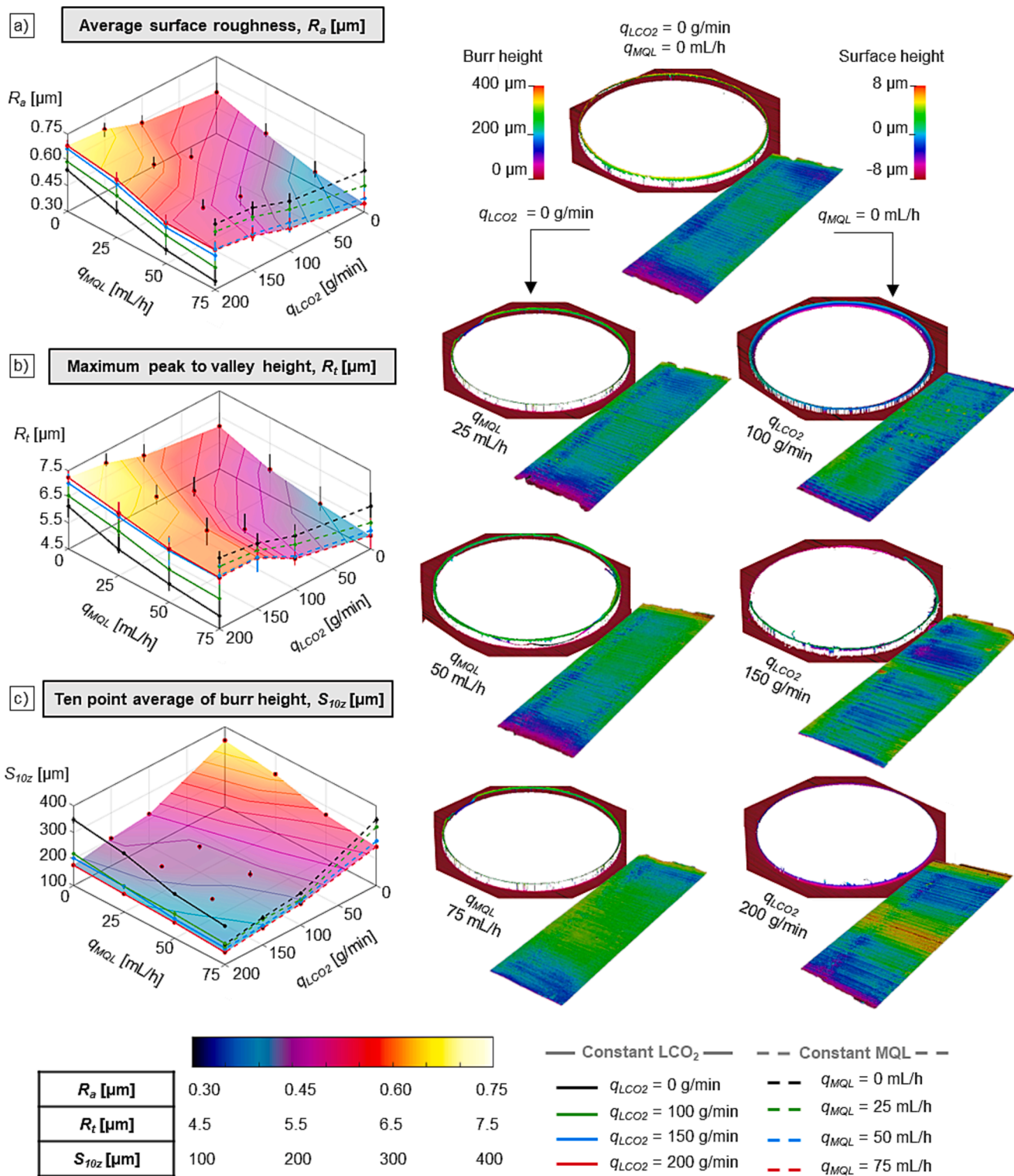


Fig. 11. Effect of varying q_{LCO_2} and q_{MQL} on hole quality when drilling Ti6Al4V individual plates: a) Average surface roughness; b) Maximum peak to valley height; c) Ten point average of burr height.

(Fig. 9b), temperatures below zero were reached in CFRP when using q_{LCO_2} above 150 g/min. Also, a considerable temperature reduction was achieved when supplying MQL without LCO₂ cooling. When drilling Ti6Al4V, the effect of the MQL on heat reduction was less pronounced. However, with LCO₂ cooling, the cutting temperature was reduced by half when LCO₂ flow rates of $q_{LCO_2} = 150$ g/min were used. In Fig. 9b the temperature fields of LCO₂ cooling show that the tool tip is considerably colder than the cutting edges, since the coolant came through the tool.

4.1.2. Hole quality in CFRP

The drilling induced push-out delamination and the surface morphology are shown in Fig. 10. As can be seen, surface roughness and voids related to fibre pull-out (Fig. 10a and b) and delamination (Fig. 10c) decreased when MQL was applied, and increased when the LCO₂ flow rate rose. Applying LCO₂ through the tool had a detrimental effect on the quality of CFRP holes. The increase in thrust force generated by the LCO₂, might have generated greater push-out delamination, as also shown by other studies [4,19]. The rise in fibre pull-out created by LCO₂ might be related to the increase in transverse elastic toughness of the epoxy matrix at low temperatures [38], in combination with the brittle fracture that governs chip formation mechanisms in composites [6]. In Fig. 10, the delaminated areas at the exit plane of the composite are marked in red in. When looking at the 3D surface morphology, a greater number of peaks (in yellow and red) and valleys (in dark blue and purple) indicate a greater number of pulled-out fibres.

4.1.3. Hole quality in Ti6Al4V

The response surfaces of R_a , R_t and burr height, as well as the surfaces measured with the Alicona Infinite Focus SL, are given in Fig. 11. LCO₂ through the tool cooling produced machined surfaces of poorer quality than when only MQL was supplied or dry machining, although the LCO₂ coolant helped to improve the hole diameter and reduce the torque. This might have occurred due to the worse tribological properties of LCO₂ [35]. On the other hand, the temperature reduction achieved by increasing q_{LCO_2} contributed to the reduction in burr height (Fig. 11c). This could be related to the damage mechanism of Ti6Al4V, which is dominated by elastoplastic deformation [6]. At lower temperatures the plasticity of the titanium decreases, thus reducing the burr height. Similar results were observed by Gao et al. [39] using VAD. When q_{MQL} increased, an improvement in both surface roughness and burr height was observed. This could be due to the reduction in torque and cutting temperature achieved by combining cooling and lubrication in the cutting zone with LCO₂ + MQL.

Table 7

Individual objectives, constraints, and weights for every output parameter employed in the multi-objective optimisation of the LCO₂ and MQL flow rates for drilling separate CFRP and Ti6Al4V plates.

	CFRP			Ti6Al4V		
Output parameter	Objective	Constraints [min – max]	wi [%]	Objective	Constraints [min – max]	wi [%]
Thrust force, F_z	Minimise	91.6 – 138.7	7.9	Minimise	533.6 – 670.6	7.8
Torque, M_z	Minimise	0.102 – 0.154	6.7	Minimise	0.952 – 1.343	13.2
Temperature, T	25 °C	-21.3 – 104.3	16.4	Minimise	187.6 – 487.9	21.3
Hole diameter, ϕ	Minimise	6.007 – 6.08	20.1	6 mm	5.99 – 6.057	4.8
Roundness, σ	-	-	-	-	-	-
Arithmetic mean height, S_a	Minimise	2.45 – 4.84	9	-	-	-
Maximum valley depth, S_v	Minimise	16.9 – 35.52	7.5	-	-	-
Delamination, F_{da}	Minimise	2.05 – 3.01	5.9	-	-	-
Matrix carbonisation	-	-	-	-	-	-
Average surface roughness, R_a	-	-	-	Minimise	0.35 – 0.682	6
Maximum peak to valley height, R_t	-	-	-	Minimise	5 – 7.24	6.6
Ten point burr height, S_{10z}	-	-	-	Minimise	129 – 248.6	13.8
LCO ₂ flow rate, q_{LCO_2}	Minimise	0 – 200	12.3	Minimise	0 – 200	12.3
MQL flow rate, q_{MQL}	Minimise	0 – 75	14.2	Minimise	0 – 75	14.2

4.1.4. Multi objective optimisation

In order to achieve optimal q_{LCO_2} and q_{MQL} values for drilling separate CFRP and Ti6Al4V plates, the output parameters listed in Table 5 for each material (cutting forces, temperatures, different hole quality

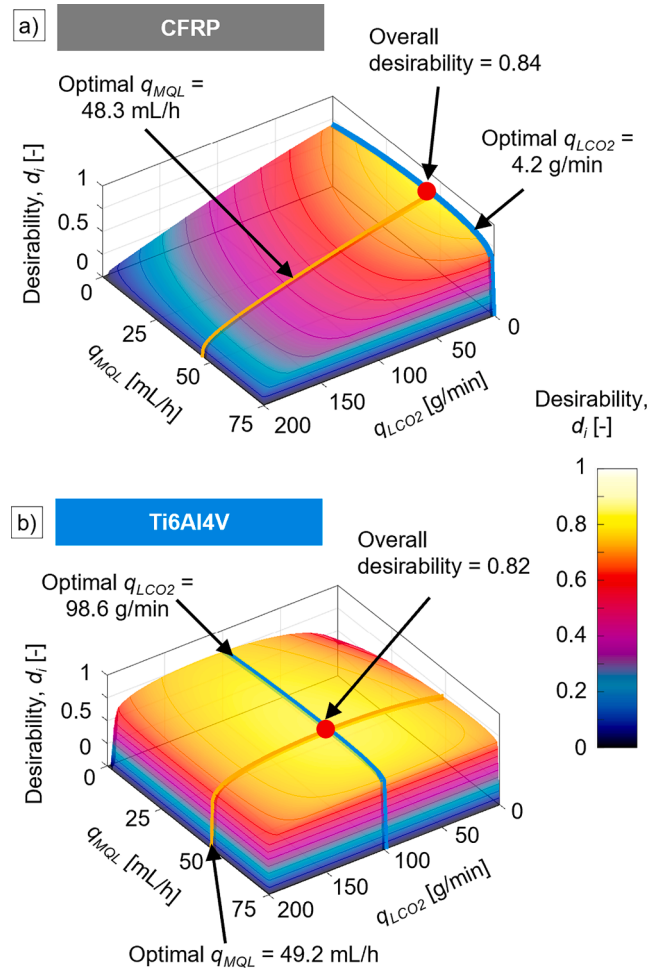


Fig. 12. Overall desirability surfaces and optimal q_{LCO_2} and q_{MQL} values for drilling: a) CFRP and b) Ti6Al4V.

Table 8

Selected cooling/lubrication parameters to test in CFRP/Ti6Al4V drilling experiments.

Experiment name	q_{LCO_2} [g/min]	q_{MQL} [mL/h]
DRY	0	0
MQL	0	50
LCO ₂	100	0
LCO ₂ + MQL	100	50

parameters depending on the material, and LCO₂ and MQL consumption), needed to meet the optimisation objectives. As seen in Table 7, the objective for most output parameters was minimisation, however, as the damage in CFRP plates increased with sub-zero temperatures, a target temperature of 25 °C was set. This way, when drilling CFRP with optimised cooling/lubrication parameters, the cutting temperature will be close to the ambient one. The constraints used for the MOO were the maximum and minimum measured values for each of the outputs. The w_i values calculated by EMW for every output are listed in Table 7.

The overall desirability surfaces for CFRP and Ti6Al4V are shown in Fig. 12. The highest desirability value corresponds to the combination of q_{LCO_2} and q_{MQL} that better satisfies all the objectives and constraints set for the different output responses in each of the materials. As it can be observed, the best results for drilling CFRP were obtained when q_{LCO_2} is very close to 0 g/min and q_{MQL} is about 50 mL/h (Fig. 12a). This configuration of cooling/lubrication parameters ensures good hole quality, while preventing the workpiece from freezing. On the other hand, when drilling Ti6Al4V, as the cutting temperature is higher, the optimal q_{LCO_2} value was around 100 g/min, while a MQL flow rate of 50

mL/h was found to be optimal (Fig. 12b).

4.2. CFRP/Ti6Al4V stacks

An experimental plan consisting of the optimized q_{LCO_2} and q_{MQL} values for drilling individual CFRP and Ti6Al4V, and two extended conditions (dry drilling and pure LCO₂ assisted drilling) was carried out on CFRP/Ti6Al4V stacks. The cooling/lubrication parameters employed for each test are detailed in Table 8.

4.2.1. Cutting forces and temperatures

Fig. 13 shows the evolution of the cutting forces and temperature of the workpiece for different cooling/lubrication techniques during the entire drilling process of the CFRP/Ti6Al4V stack. The maximum temperature profile was acquired by recording the temperature through the pilot hole (Fig. 6c). Similar to the individual plate drilling experiments, an increase in F_z was observed when applying LCO₂ (Fig. 13c and d), in comparison to DRY and MQL cases (Fig. 13a and b). Supplying LCO₂ also increased M_z in the CFRP phase, while reducing it when the drill was machining through the Ti6Al4V due to better chip evacuation and reduced thermal shrinkage [20,36]. The cutting temperature was considerably lower for the LCO₂ and LCO₂ + MQL cases (Fig. 13c and d), showing that the cutting temperature when CFRP/Ti6Al4V stack drilling can be reduced by half when delivering LCO₂ through the tool.

The temperature fields recorded from the side of the stack shown in Fig. 14, revealed that the titanium chips heated up the CFRP phase while being evacuated. This temperature value was similar or higher than the glass transition temperature of the epoxy matrix (180 °C) in DRY and MQL conditions (Fig. 14a and b), which increases the risk of matrix

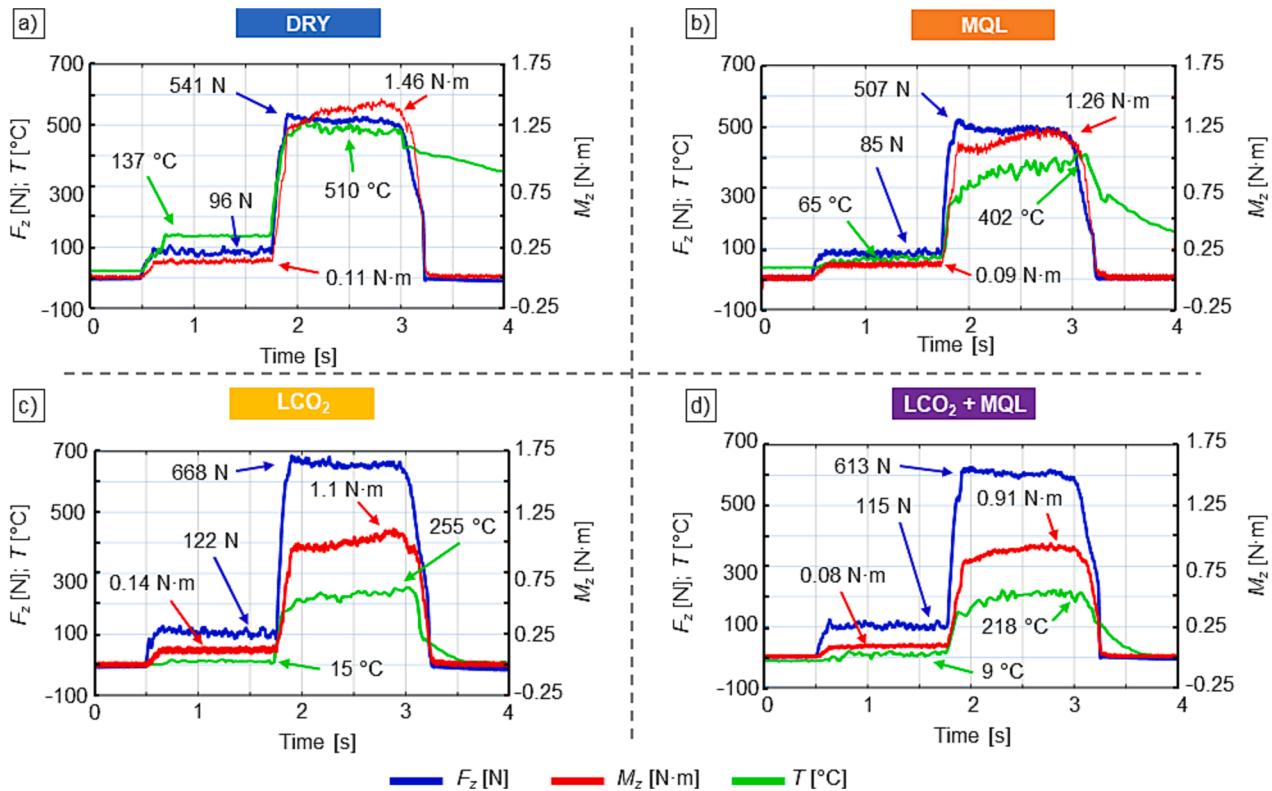


Fig. 13. Cutting force and temperature evolution when drilling CFRP/Ti6Al4V stacks under different cooling/lubrication conditions: a) DRY; b) MQL; c) LCO₂; d) LCO₂ + MQL.

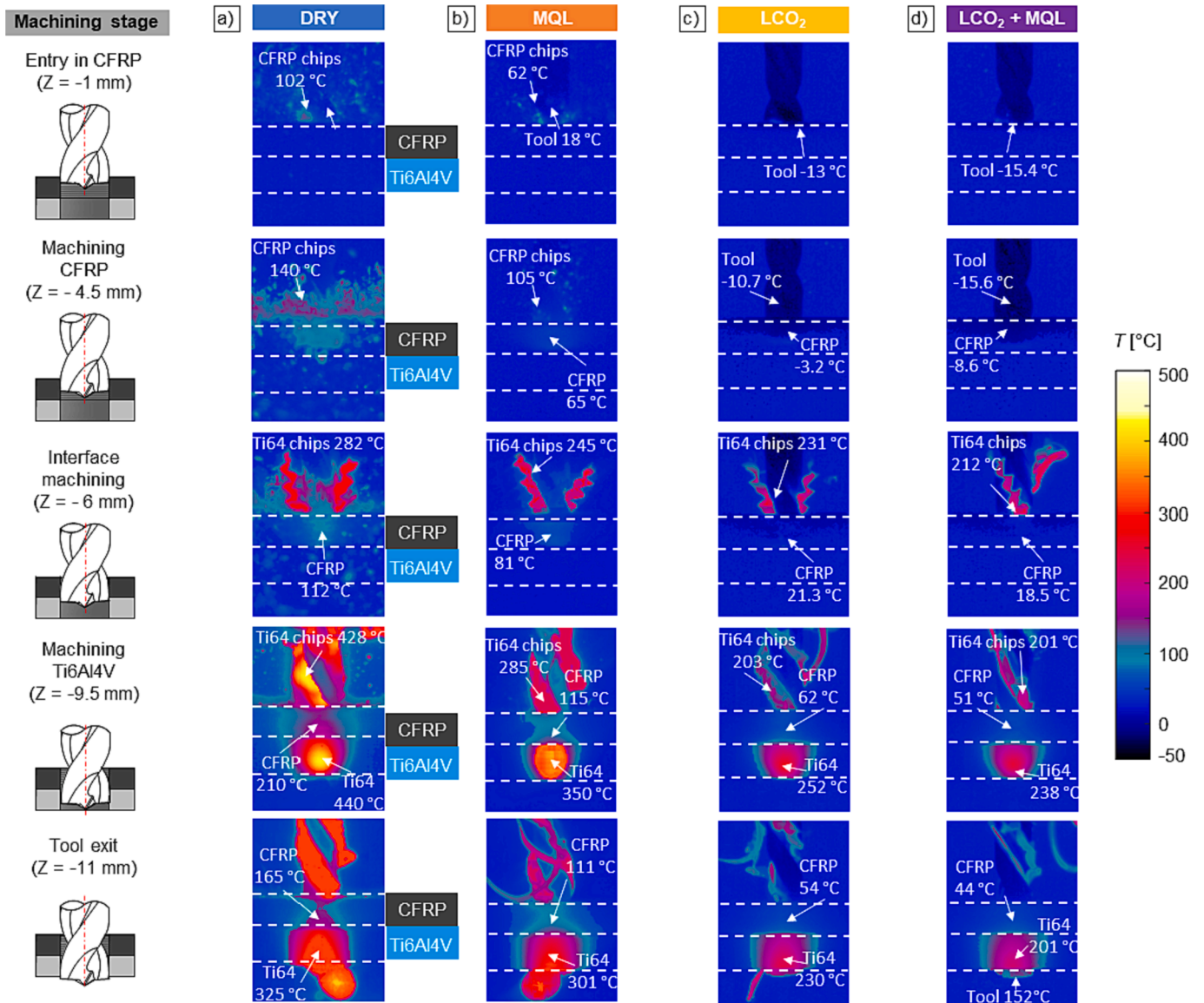


Fig. 14. Temperature fields when drilling CFRP/Ti6Al4V stacks under different cooling/lubrication conditions: a) DRY; b) MQL; c) LCO₂; d) LCO₂ + MQL.

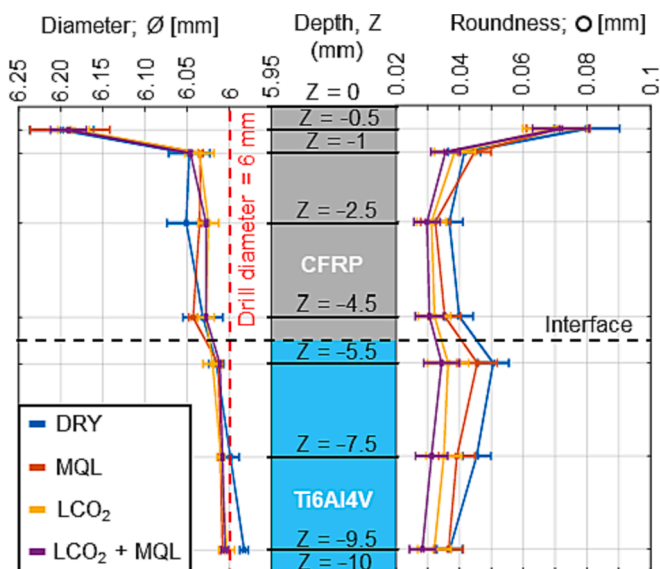


Fig. 15. Dimensional accuracy of holes drilled in CFRP/Ti6Al4V stacks under different cooling/lubrication conditions.

carbonisation as demonstrated by [38]. For LCO₂ and LCO₂ + MQL conditions (Fig. 14c and d), the temperature of the Ti6Al4V chips was considerably lower. As a result, the temperature of the CFRP and risk of matrix carbonisation decreased, but without reaching freezing temperatures. This could be due to the heat generated as the Ti6Al4V plate is being machined.

4.2.2. Hole quality in CFRP/Ti6Al4V stacks

The hole diameter and roundness obtained at eight depths, with the different cooling/lubrication techniques, are shown in Fig. 15. The error in roundness and diameter is the greatest at the entry of the CFRP phase, which is due to the delamination of the first plies of the laminate creating an irregular surface in the first microns of depth. The reduction in cutting temperature due to LCO₂ cooling contributed to decrease the thermal shrinkage in titanium and improve the hole roundness and accuracy in the stack.

In Fig. 16 the different hole quality parameters analysed, and their location in the CFRP/Ti6Al4V stack can be seen. Peel-up delamination was greater when using LCO₂ cooling (Fig. 16a), probably due to an

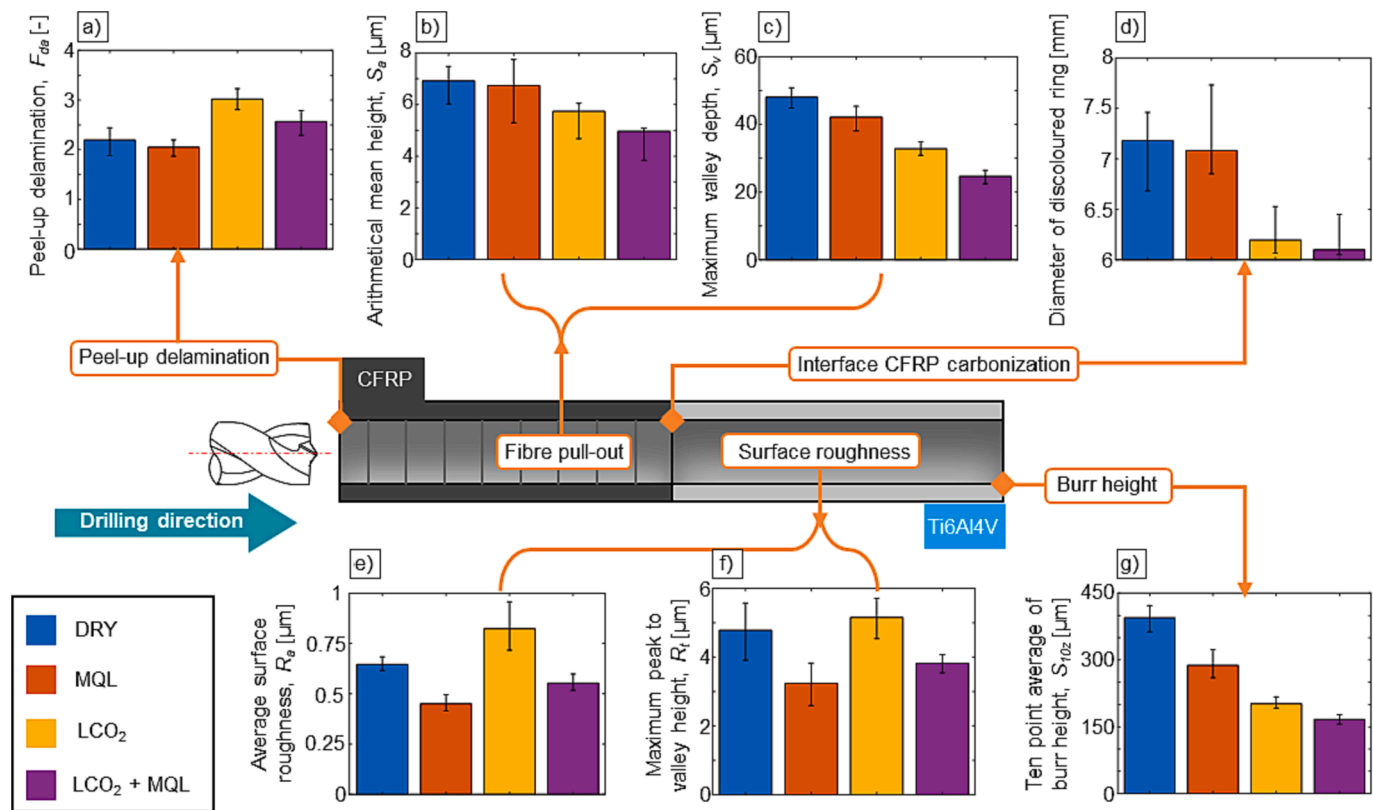


Fig. 16. Evaluation of hole quality of CFRP and Ti6Al4V phases when drilling stacks under different cooling/lubrication conditions.

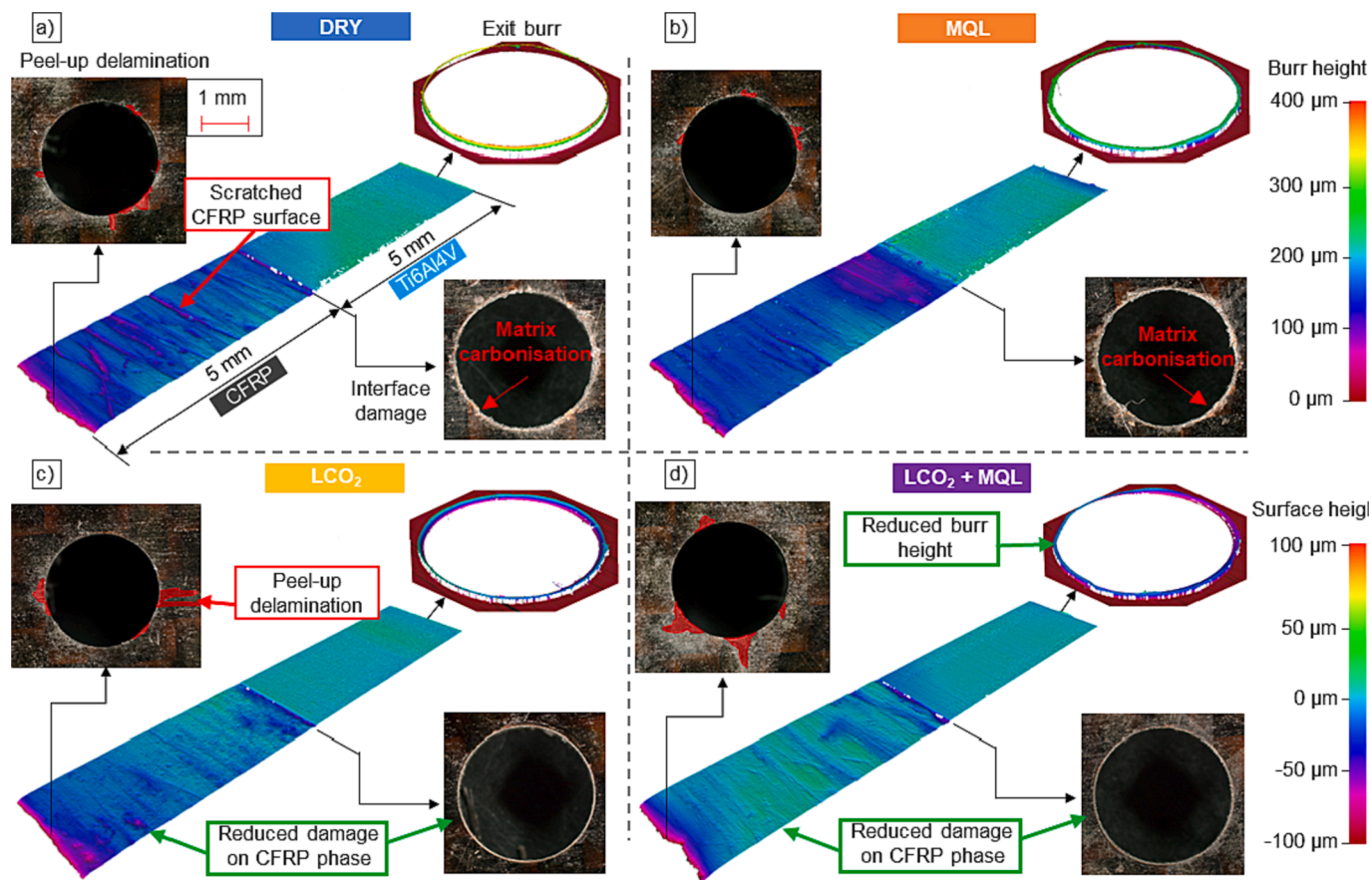


Fig. 17. Visual comparison of hole quality of CFRP and Ti6Al4V phases when drilling stacks under different cooling/lubrication conditions: a) DRY; b) MQL; c) LCO₂; d) LCO₂ + MQL.

increase in the thrust force. However, using through the tool LCO₂, greatly improved the surface roughness (S_a) and reduced the voids (S_v), which are related to fibre pull-out (Fig. 16b and c). This could be due to an improvement in titanium chip evacuation by the LCO₂, which reduced thermal and mechanical damage produced by the chips on the machined CFRP surface. CFRP matrix carbonisation at the interface (Fig. 16d) was also greatly reduced when using LCO₂ and LCO₂ + MQL. This was expected as lower temperatures were recorded at the CFRP phase for these cooling/lubrication cases (Fig. 14c and d). The hole quality in the Ti6Al4V phase of the stack followed the same trend as for individual titanium plates (Fig. 11). Surface roughness was improved when using MQL lubrication (Fig. 16e and f), and the burr height was reduced due to the cold temperatures of LCO₂ (Fig. 16g).

In Fig. 17 the visual comparison of the hole quality is shown. The damage on CFRP phase by titanium chips, as well as the matrix carbonisation is clear for DRY and MQL cases (Fig. 17a and b), since the cutting temperature was higher, and the titanium chip evacuation was worse. For LCO₂ and LCO₂ + MQL cases (Fig. 17c and d), less scratches and carbonisation are observed on the CFRP. No push-out delamination was observed at the exit of the CFRP, due to the support provided by the Ti6Al4V.

5. Conclusions

The present work analyses the effect of LCO₂ and MQL flow rates, and defines the optimal values for drilling CFRP, Ti6Al4V and CFRP/Ti6Al4V stacks, by performing a multi-objective optimisation of cutting forces, temperature, and various hole quality parameters. The conclusions are as follows:

- The results show that LCO₂ cooling is detrimental for drilling CFRP plates, since the cutting temperature was not critical. Pure MQL lubrication produced the best hole quality, as it lubricated the cutting zone without freezing it. On the other hand, for Ti6Al4V and CFRP/Ti6Al4V stack drilling using LCO₂ + MQL at $q_{LCO_2} = 100$ g/min and $q_{MQL} = 50$ mL/h achieved the best results. When drilling stacks, the cooling and lubrication by LCO₂ + MQL helped to reduce the thermal damage in the CFRP phase and the burr height in the Ti6Al4V.
- Supplying LCO₂ + MQL through the tool created a decrease in the torque due to better chip evacuation and reduced hole shrinkage when drilling Ti6Al4V individually and in the stack. On the downside, LCO₂ cooling increased the flow stress of the workpiece material, and thus the thrust force. However, this effect was reduced when adding MQL to the LCO₂.
- Machining stacks in the direction from CFRP to Ti6Al4V resulted in suppression of delamination defects in the CFRP phase. LCO₂ + MQL supplied through the tool significantly reduced the degradation of the machined CFRP surface by improving evacuation of the titanium chips and reducing the cutting temperature. Additionally, the burr height of the titanium was also reduced due to the decrease in plastic deformation of the workpiece promoted by LCO₂ cooling.
- Future efforts should focus on varying the flow rate of LCO₂ + MQL during the process to provide the optimum mix of coolant at every stage of the machining operation. However, limitations in the time required to stabilize the LCO₂ + MQL flow rate should be considered.

Funding sources

This research was financially supported by the ARRS – national science agency within research program 2–0266 (Advanced manufacturing technologies for high quality and sustainable production), and the projects CRYOMACH (INNO-20182049) from Smart Advanced Manufacturing call, OPTICED (KK-2021/00003) from Elkartek call, and EIT Manufacturing: Transitioning to a waste-free production – international cryogenic + MQL machining activity (2021, 2023).

CRedit authorship contribution statement

I. Rodríguez: Conceptualization, Methodology, Validation, Investigation, Writing – original draft. **P.J. Arrazola:** Conceptualization, Supervision, Project administration, Funding acquisition, Writing – review & editing. **M. Cuesta:** Conceptualization, Supervision, Project administration, Writing – review & editing. **F. Pušavec:** Conceptualization, Supervision, Project administration, Funding acquisition, Writing – review & editing.

Declaration of Competing Interest

The authors declare that they have no known competing financial interests or personal relationships that could have appeared to influence the work reported in this paper.

Data availability

The data that has been used is confidential.

Acknowledgements

The authors would like to express their great appreciation to SECO Tools for providing the tools necessary to carry out this research work.

References

- [1] ACARE, "Flightpath 2050 Europe's vision for aviation: Report of the high level group on aviation research," 2011. doi: 10.2777/50266.
- [2] Xu J, Mkaddem A, El Mansori M. Recent advances in drilling hybrid FRP/Ti composite: A state-of-the-art review. *Compos Struct* 2016;135:316–38. <https://doi.org/10.1016/j.compstruct.2015.09.028>.
- [3] Xu J, Li C, Chen M, El Mansori M, Davim JP. On the analysis of temperatures, surface morphologies and tool wear in drilling CFRP/Ti6Al4V stacks under different cutting sequence strategies. *Compos Struct* 2020;234:111708. <https://doi.org/10.1016/j.compstruct.2019.111708>.
- [4] Geier N, Davim JP, Szalay T. Advanced cutting tools and technologies for drilling carbon fibre reinforced polymer (CFRP) composites: A review. *Compos A Appl Sci Manuf* 2019;125:105552. <https://doi.org/10.1016/j.compositesa.2019.105552>.
- [5] Shah P, Khanna N, Singla AK, Bansal A. Tool wear, hole quality, power consumption and chip morphology analysis for drilling Ti-6Al-4V using LN2 and LCO₂. *Tribol Int* 2021;163:107190. <https://doi.org/10.1016/j.triboint.2021.107190>.
- [6] Xu J, Lin T, Li L, Ji M, Davim JP, Geier N, Chen M. Numerical study of interface damage formation mechanisms in machining CFRP/Ti6Al4V stacks under different cutting sequence strategies. *Compos Struct* 2022;285:115236. <https://doi.org/10.1016/j.compstruct.2022.115236>.
- [7] Pecat O, Brinksmeier E. Low damage drilling of CFRP/titanium compound materials for fastening. *Procedia CIRP* 2014;13:1–7. <https://doi.org/10.1016/j.procir.2014.04.001>.
- [8] Lazoglu I, et al. Thermal analysis in Ti-6Al-4V drilling. *CIRP Ann - Manuf Technol* 2017;66(1):105–8. <https://doi.org/10.1016/j.cirp.2017.04.020>.
- [9] Cao S, et al. Investigation of CFRP damages induced by the interface high temperature and mixed tool wear mechanism in drilling of thin-walled CFRP / Ti stacks. *Compos Struct* 2022;323:2023.
- [10] Xu J, Li C, Chen M, Ren F. A comparison between vibration assisted and conventional drilling of CFRP/Ti6Al4V stacks. *Mater Manuf Process* 2019;34(10):1182–93. <https://doi.org/10.1080/10426914.2019.1615085>.
- [11] Jiao F, Li Y, Niu Y, Zhang Z, Bie W. A review on the drilling of CFRP/Ti stacks: Machining characteristics, damage mechanisms and suppression strategies at stack interface. *Compos Struct* 2022;305:2023. <https://doi.org/10.1016/j.compstruct.2022.116489>.
- [12] Shu L, et al. Study on dedicated drill bit design for carbon fiber reinforced polymer drilling with improved cutting mechanism. *Compos A Appl Sci Manuf* 2020;142:2021. <https://doi.org/10.1016/j.compositesa.2020.106259>.
- [13] Hussein R, Sadek A, Elbestawi MA, Attia MH. Low-frequency vibration-assisted drilling of hybrid CFRP/Ti6Al4V stacked material. *Int J Adv Manuf Technol* 2018;98(9–12):2801–17. <https://doi.org/10.1007/s00170-018-2410-2>.
- [14] Li C, Xu J, Chen M, An Q, El Mansori M, Ren F. Tool wear processes in low frequency vibration assisted drilling of CFRP/Ti6Al4V stacks with forced air-cooling. *Wear* 2019;426:1616–23. <https://doi.org/10.1016/j.wear.2019.01.005>.
- [15] Sadek A, Meshreki M, Attia MH. Characterization and optimization of orbital drilling of woven carbon fiber reinforced epoxy laminates. *CIRP Ann - Manuf Technol* 2012;61(1):123–6. <https://doi.org/10.1016/j.cirp.2012.03.089>.
- [16] Turner J, Scaife RJ, El-Desouky HM. Effect of machining coolant on integrity of CFRP composites. *Adv Manuf Polym Compos Sci* 2015;1(1):54–60. <https://doi.org/10.1179/2055035914Y.0000000008>.

- [17] Pereira O, Rodríguez A, Fernández-Abia AI, Barreiro J, López de Lacalle LN. Cryogenic and minimum quantity lubrication for an eco-efficiency turning of AISI 304. *J Clean Prod* 2016;139:440–9. <https://doi.org/10.1016/j.jclepro.2016.08.030>.
- [18] Jamil M, et al. Influence of CO₂-snow and subzero MQL on thermal aspects in the machining of Ti-6Al-4V. *Appl Therm Eng* 2020;177:115480. <https://doi.org/10.1016/j.applthermaleng.2020.115480>.
- [19] Xia T, Kaynak Y, Arvin C, Jawahir IS. Cryogenic cooling-induced process performance and surface integrity in drilling CFRP composite material. *Int J Adv Manuf Technol* 2016;82(1–4):605–16. <https://doi.org/10.1007/s00170-015-7284-y>.
- [20] Merzouki J, Poulachon G, Rossi F, Ayed Y, Abrivard G. Effect of cryogenic assistance on hole shrinkage during Ti6Al4V drilling. *Int J Adv Manuf Technol* 2020;108(9–10):2675–86. <https://doi.org/10.1007/s00170-020-05381-z>.
- [21] Grguraš D, Sterle L, Krajnik P, Pušavec F. A novel cryogenic machining concept based on a lubricated liquid carbon dioxide. *Int J Mach Tool Manu Oct*. 2019;145. <https://doi.org/10.1016/j.ijmachtools.2019.103456>.
- [22] “Transitioning to a waste-free production – international cryogenic+MQL machining activity - EIT Manufacturing.” <https://www.eitmanufacturing.eu/news-events/activities/transitioning-to-a-waste-free-production-international-cryogenic-mql-machining-activity/> (accessed Oct. 11, 2023).
- [23] Rodríguez I, Arrazola PJ, Cuesta M, Sterle L, Pušavec F. Improving surface integrity when drilling CFRPs and Ti-6Al-4V using sustainable lubricated liquid carbon dioxide. *Chinese J Aeronaut* 2023;36(7):129–46. <https://doi.org/10.1016/j.cja.2022.09.004>.
- [24] Grguraš D, Sterle L, Malneršič A, Kastelic L, Courbon C, Pušavec F. Media flow analysis of single-channel pre-mixed liquid CO₂ and MQL in sustainable machining. *Stroj Vestnik/Journal Mech Eng* 2021;67(1–2):3–10. <https://doi.org/10.5545/sv-jme.2020.7076>.
- [25] Kacalak W, Lipiński D, Różański R, Królczyk GM. Assessment of the classification ability of parameters characterizing surface topography formed in manufacturing and operation processes. *Measurement* 2020;170:2021. <https://doi.org/10.1016/j.measurement.2020.108715>.
- [26] Arola D, Williams CL. Estimating the fatigue stress concentration factor of machined surfaces. *Int J Fatigue* 2002;24:923–30. [https://doi.org/10.1016/S0142-1123\(02\)00012-9](https://doi.org/10.1016/S0142-1123(02)00012-9).
- [27] Duboust N, Watson M, Marshall M, O'Donnell GE, Kerrigan K. Towards intelligent CFRP composite machining: Surface analysis methods and statistical data analysis of machined fibre laminate surfaces. *Proc Inst Mech Eng Part B J Eng Manuf* 2021; 235(10):1602–17. <https://doi.org/10.1177/0954405420960920>.
- [28] Segurajaregui U, Arrazola PJ. Heat-flow determination through inverse identification in drilling of aluminium workpieces with MQL. *Prod Eng Res Dev* 2015;9(4):517–26. <https://doi.org/10.1007/s11740-015-0631-x>.
- [29] Telops Inc., “Telops Infrared Camera Blackbody-Free Calibration Technique.” http://info.telops.com/Website-content-requests_05—LP—Infrared-Camera-Blackbody-Free-Calibration-Technique.html (accessed Mar. 29, 2022).
- [30] Fu R, et al. Drill-exit temperature characteristics in drilling of UD and MD CFRP composites based on infrared thermography. *Int J Mach Tool Manu* 2018;135: 24–37. <https://doi.org/10.1016/j.ijmachtools.2018.08.002>.
- [31] Sela A, Ortiz-de-zarate G, Soler D, Germain G, Gallegos L, Arrazola PJ. International Journal of Heat and Mass Transfer Adiabatic self-heating determination for Ti6Al4V at different temperatures. *Int J Heat Mass Transf* 2023; 204:123747. <https://doi.org/10.1016/j.ijheatmasstransfer.2022.123747>.
- [32] Davim JP, Rubio JC, Abrao AM. A novel approach based on digital image analysis to evaluate the delamination factor after drilling composite laminates. *Compos Sci Technol* 2007;67:1939–45. <https://doi.org/10.1016/j.compscitech.2006.10.009>.
- [33] Kumar R, et al. Revealing the benefits of entropy weights method for multi-objective optimization in machining operations: A critical review. *J Mater Res Technol* 2021;10(4):1471–92. <https://doi.org/10.1016/j.jmrt.2020.12.114>.
- [34] Ueda T, Nozaki R, Hosokawa A. Temperature measurement of cutting edge in drilling -Effect of Oil Mist-. *CIRP Ann - Manuf Technol* 2007;56(1):93–6. <https://doi.org/10.1016/j.cirp.2007.05.024>.
- [35] Pušavec F, Sterle L, Kalin M, Mallipeddi D, Krajnik P. Tribology of solid-lubricated liquid carbon dioxide assisted machining. *CIRP Ann* 2020;69:69–72. <https://doi.org/10.1016/j.cirp.2020.04.033>.
- [36] Sterle L, Krajnik P, Pušavec F. The effects of liquid-CO₂ cooling, MQL and cutting parameters on drilling performance. *CIRP Ann* 2021;70(1):79–82. <https://doi.org/10.1016/j.cirp.2021.04.007>.
- [37] Xu J, Lin T, Davim JP. On the Machining Temperature and Hole Quality of CFRP Laminates when Using Diamond-Coated Special Drills. *J Compos Sci* 2022;6(2): 1–14. <https://doi.org/10.3390/jcs6020045>.
- [38] Kubher S, Gururaja S, Zitoun R. Coupled thermo-mechanical modeling of drilling of multi-directional polymer matrix composite laminates. *Compos. Part A Appl. Sci. Manuf.* 2022;156:106802. <https://doi.org/10.1016/j.compositesa.2022.106802>.
- [39] Gao G, Xia Z, Yuan Z, Xiang D, Zhao B. Influence of longitudinal-torsional ultrasonic-assisted vibration on micro-hole drilling Ti-6Al-4V. *Chinese J Aeronaut* 2021;34(9):247–60. <https://doi.org/10.1016/j.cja.2020.06.012>.
- [40] Sadek A, Attia MH, Meshreki M, Shi B. Characterization and optimization of vibration-assisted drilling of fibre reinforced epoxy laminates. *CIRP Ann - Manuf Technol* 2013;62(1):91–4. <https://doi.org/10.1016/j.cirp.2013.03.097>.
- [41] Sun Z, Geng D, Meng F, Zhou L, Jiang X. High performance drilling of T800 CFRP composites by combining ultrasonic vibration and optimized drill structure. *Ultrasonics* 2023;134:107097. <https://doi.org/10.1016/j.ultras.2023.107097>.
- [42] Shao Z, et al. The interface temperature and its influence on surface integrity in ultrasonic-assisted drilling of CFRP/Ti stacks. *Compos Struct* 2021;266:113803. <https://doi.org/10.1016/j.compstruct.2021.113803>.
- [43] Bleicher F, Wiesinger G, Kumpf C, Finkeldei D, Baumann C, Lechner C. Vibration assisted drilling of CFRP/metal stacks at low frequencies and high amplitudes. *Prod Eng Res Devel* 2018;12(2):289–96. <https://doi.org/10.1007/s11740-018-0818-z>.
- [44] Pan Z, Wang L, Fang Q, Sun Z, Qu W. Study on tool deflection compensation method based on cutting force observer for orbital drilling of CFRP/Ti stacks. *J Manuf Process* 2022;75:450–60. <https://doi.org/10.1016/j.jmapro.2021.12.058>.
- [45] Kong L, Gao D, Lu Y, Zhang P. Experimental investigation on machining performance during orbital drilling of CFRP. *Int J Adv Manuf Technol* 2022;121(3–4):1611–21. <https://doi.org/10.1007/s00170-022-09437-0>.
- [46] Senthilkumar M, Prabukarthi A, Krishnaraj V. Machining of CFRP/Ti6Al4V stacks under minimal quantity lubricating condition. *J Mech Sci Technol* 2018;32(8): 3787–96. <https://doi.org/10.1007/s12206-018-0731-6>.
- [47] Xu J, Ji M, Chen M, El Mansori M. Experimental investigation on drilling machinability and hole quality of CFRP/Ti6Al4V stacks under different cooling conditions. *Int J Adv Manuf Technol* 2020;109(5–6):1527–39. <https://doi.org/10.1007/s00170-020-05742-8>.
- [48] Fernández-Pérez J, Cantero JL, Díaz-Álvarez J, Miguélez MH. Hybrid composite-metal stack drilling with different minimum quantity lubrication levels. *Materials* 2019;12(3):448. <https://doi.org/10.3390/ma12030448>.
- [49] Iqbal A, et al. Between-the-holes cryogenic cooling of the tool in hole-making of Ti-6Al-4V and CFRP. *Materials (Basel)* 2021;14(4):1–19. <https://doi.org/10.3390/ma14040795>.
- [50] Rodríguez A, Calleja A, de Lacalle LL, Pereira O, Rubio-Mateos A, Rodríguez G. Drilling of CFRP-Ti6Al4V stacks using CO₂-cryogenic cooling. *J. Manuf. Process.* 2021;64:58–66. <https://doi.org/10.1016/j.jmapro.2021.01.018>.